AD-A038 350 HUGHES AIRCRAFT CO CULVER CITY CALIF ANTENNA DEPT F/G 17/9
CONFORMAL PHASED ARRAY BREADBOARD.(U)
JAN 77 P C BARGELIOTES, A F SEATON N00019-76-C-0495
UNCLASSIFIED 2753/981 NL

1 OF 1
AD A038350

END
DATE FILMED
5-77

HAC REF. NO. D61
DEPT. REF. 2753/9

(12)

See 1473

Contract N00019-76-C-0495

CONFORMAL PHASED ARRAY BREADBOARD

FINAL REPORT

JANUARY 1977

**Prepared for the AIR SYSTEMS COMMAND
Department of the NAVY**

ANTENNA DEPARTMENT

HUGHES

RADAR SYSTEMS GROUP
HUGHES AIRCRAFT COMPANY
CULVER CITY, CA 90230

Reference No. 2753/981

HAC Reference D6190

CONFORMAL PHASED ARRAY BREADBOARD

CONTRACT N00019-76-C-0495

FINAL REPORT

January 1977

Prepared by

P.C. Bargeliotes
A.F. Seaton
A.T. Villeneuve
and
W.H. Kummer
Antenna Department
Radar Microwave Laboratory

Prepared for

Air Systems Command
Department of the Navy
Washington, D.C.

Engineering Division
Radar Systems Group
Hughes Aircraft Company • Culver City, California

TABLE OF CONTENTS

LIST OF ILLUSTRATIONS

LIST OF TABLES

ACKNOWLEDGEMENTS

The following personnel of the Antenna Department in the Radar Systems Group of the Hughes Aircraft Company contributed to the Conformal Phased Array Breadboard program during the period covered by the contract:

Dr. W. H. Kummer	Program Manager, Chief Scientist
Dr. P. C. Bargeliotes	Staff Engineer
Mr. N. C. Olsen	Staff Physicist
Mr. A. F. Seaton	Senior Staff Engineer
Dr. A. T. Villeneuve	Senior Scientist

During this program several technical exchanges occured between the personnel performing on the program and Drs. S.W. Lee (UI), R. Mittra (UI) and R.C. Hansen (consultant). These meetings were fruitful and technically stimulating.

The technical officer for this program is Mr. J.W. Willis (AIR-310B).

1.0 INTRODUCTION

For missile seeker radars, the use of mechanically scanned antenna systems becomes increasingly difficult as the requirements for the aerodynamic and electrical performance of missiles become more demanding. One possible alternative to the use of mechanically scanned antennas lies in the direction of flush-mounted slot antenna systems on metallic cones or ogival surfaces. These antenna systems would be inertialessly scanned in the required directions. Since scanning over a wide angular region is desired, the radiation characteristics, including the effects of mutual coupling on the radiating elements, must be investigated before the more detailed system aspects are considered. Those aspects of the problems that involve the antenna radiation characteristics have been examined.

For the purposes of this program, representative radiators integral with the surface of a 20° full angle cone were chosen as the model. The study has included a theoretical investigation of the radiation characteristics of circumferential and radial slots on the cone. X-band was chosen as the system frequency.

Exact modal analyses have been implemented to compute patterns of circumferential and radial slots on cones. The computed patterns have shown excellent agreement with measurement of an experimental model with both types of slots. The relatively slow convergence of the modal series and associated computational difficulties, however, limit the applicability of the technique to slots relatively close to the tip of the cone. In addition to the exact technique, various approximation techniques have been examined for use in pattern calculations and in impedance calculations. These

include the approximate asymptotic approach and the equivalence principle technique. The approximation techniques provide simplified computations as compared with the exact technique, and are not applicable to all conditions. A combination of exact and approximation techniques is generally required to design or analyze an array.

The approximate asymptotic approach, which allows the separation of the diffracted field and geometrical optics field, has been examined in detail and the results were presented in the Final Report on Contract No. N00019-74-C-0127 (Bargeliotes, Villeneuve, and Kummer, 1975) and Final Report on Contract No. N00019-75-C-0160 (Bargeliotes, Villeneuve, and Kummer, 1976). The investigation of the technique has been continued during this period. It appears that the asymptotic representation of the Legendre function chosen for the analysis leads to divergent expressions as the mode number m is increased, and hence limits the usefulness of the asymptotic approach in the present problem. The computed radiation patterns of several azimuthal modes presented in Section 2 verify the divergent nature of the asymptotic expression.

The direct synthesis of radiation patterns of arrays on conical or other more generally curved surfaces is a difficult problem. However, the application of an equivalence principle allows the synthesis to be carried out by using a convenient reference source located within the curved surface and by determining the fields of the reference source over that surface. From these fields equivalent sources on the surface can be determined. A computer program is being developed to apply this technique to a conical surface. The new program will employ an improved element pattern over versions with an array lattice identical to that used by the companion program for phase and polarization quantization.

Radiation patterns from slot configurations on cones have also been computed by a conical array computer program in which continuously variable phase shifts and continuously rotatable polarization have been introduced. Since real devices are usually digital in nature, digital devices appear to be likely candidates for use in a practical conical array. Accordingly, the computer program was modified to employ digital phase and polarization control and a series of patterns were computed and compared with those obtained for the continuously variable case.

The design of a conformal array on a cylindrical or a conical surface requires knowledge of the mutual admittance of slots on such surfaces. Expressions for mutual coupling of dominant mode slots on a conducting cylinder suitable for numerical computations have been found by the harmonic series by Golden, Stewart and Pridmore-Brown (1974). Since the harmonic series results in precise calculations of mutual coupling for the cylinder, the cylinder is taken as the test model for other configurations.

For example, Golden, et al., have extended the harmonic series analysis of the cylinder to predict mutual coupling of slots on a conical surface for certain geometries. This is done by adding the tip-diffraction effects of the cone tip to results obtained from an equivalent cylindrical model of the slots on the conical surface. The equivalent cylinder has a radius equal to the radius of the circular cross section of the cone midway between the two slot antennas.

The harmonic series as formulated by Golden, et al., contains a non-integrable singularity and in actual numerical calculations a small loss tangent must be assumed in the expressions for the propagation constant for free space. The applicability of the harmonic series is also limited to

relatively small axial slot separations since the expression is highly oscillatory for large slot separations. An alternative modal solution for mutual admittance has been obtained by Lee (1976) from the harmonic series, cast in a form that does not require the introduction of small loss. The integrand of the alternative modal expansion decays exponentially for large slot separations instead of being highly oscillatory; however, the expansion is not valid when the axial separation of the slots is zero. Thus the self-admittance cannot be obtained. Preliminary calculations using the alternative modal expansion indicate excellent agreement with the harmonic series calculations even for small axial slot separations.

2.0 RADIATION PATTERNS OF SLOTS ON CONES

Radiation patterns of circumferential slots on cones have been computed by the exact modal series and are used to check the accuracy of computation of similar radiation patterns by approximate methods. The approximate asymptotic approach, for example, allows the separation of the diffracted field and the geometrical optics field. The diffraction field is expressed in terms of diffraction coefficients which are only a function of the angular coordinates and do not depend on the radial location of the radiating element. The diffraction field of any element location is found by taking the product of the diffraction coefficients and a simple factor containing the information about the location of the radiating element. In the following sections, computed total and mode radiation patterns from the approximate asymptotic approach are compared with corresponding patterns from the normal mode series. The application of the equivalence principle in radiation pattern computation is also discussed. In section 2.3, the effect of phase and polarization quantization on the performance of a conical array are presented.

2.1 Mode Fields of Circumferential Slots on a Cone

The total radiation patterns of the modal series have been compared with measurement data of an experimental model and are in good agreement. The modal series radiation patterns were also compared with corresponding patterns from the asymptotic method and showed good agreement as long as only the first few modes of the asymptotic method were summed. As more modes were considered in the computations, the values for the fields from the asymptotic method increased rapidly over most of the range of θ, rendering

the asymptotic method quite inaccurate. After further computations and examination of the asymptotic field expressions, it became evident that all three types of fields (optical, transition and diffracted) diverge with increasing mode number. This behavior precludes the accurate computation of patterns by redefining the diffraction coefficients or eliminating the diffraction coefficients and corresponding singularities of the transition fields for higher order modes altogether. Since the modal field is obtained by summing the optical, the transition and the diffracted fields for each mode, the optical field must also be convergent with $\underline{m}$ if the approximate mode field is to be identical to the normal mode series mode field of the same mode. However, it may still be possible to use the diffraction and transition fields of the first few modes and to neglect the remaining modes. It may then be possible to combine these diffraction and transition fields of the first few modes with the results of the geometrical theory of diffraction to obtain approximate patterns. The reason for this may be seen by examining the exact modal fields. It is apparent that the effects of diffraction are significant only in the first few modes and the exact modal fields themselves decrease rapidly in the transition region ($\theta \approx \pi - \theta_o$). Therefore, the higher order diffraction and transition modes are not significant. Thus they may be neglected, and the fact that the asymptotic expressions for these fields give incorrect results does not matter, since it is not necessary to use them to approximate the radiation patterns.

The exact modal fields were examined by observing the relative magnitude of each mode prior to sequential summation. The unnormalized mode fields of the first few modes of the modal series are shown in Figures 2

and 3 for the θ-polarization and Figures 4 and 5 for the φ-polarization.(A) For the E_θ component the mode field drops off quite rapidly as m increases and is of significance only at the broadside region (θ = 80°). The m = 5 mode, for example, has an average value of about -24 dB from θ = 40° to θ =140° and about 1 dB ripple from θ = 40° to θ = 70°. Outside this range of theta, this mode contributes very little to the total field. Likewise, the effect of the higher order modes becomes less important except near the broadside region. Thus, the higher order modes can be eliminated from the computations completely, except, perhaps, at the broadside region. The E_ϕ component mode fields show similar sharp drop-off as the E_θ component near the $\theta = \pi - \theta_o$ and near the $\theta = \theta_o$ regions. All modes show a minimum in the vicinity of θ = 90°. Below θ = 25°, the contribution of the modes to the total field is decreasing with increasing mode number m. At θ = 165°, the m = 3 mode seems to contribute the greatest amount to the total field. The m = 7 mode is at a level of approximately -30 dB throughout the whole range of θ.

In Figures 3 and 5, the mode field of m = 9 as computed from the asymptotic expressions is also shown for the E_θ and E_ϕ components, respectively. It is evident from the curves that the E_θ mode field from the asymptotic expressions is approximately 25 dB avove the modal series field at the broadside region and considerably higher everywhere else. Similar behavior is noted for the E_ϕ mode fields of Figure 5 except the difference between the two different patterns at the broadside region is not as great. Mode fields from the asymptotic expressions were also computed with only the

(A) The usual spherical coordinate system is employed as shown in Figure 1.

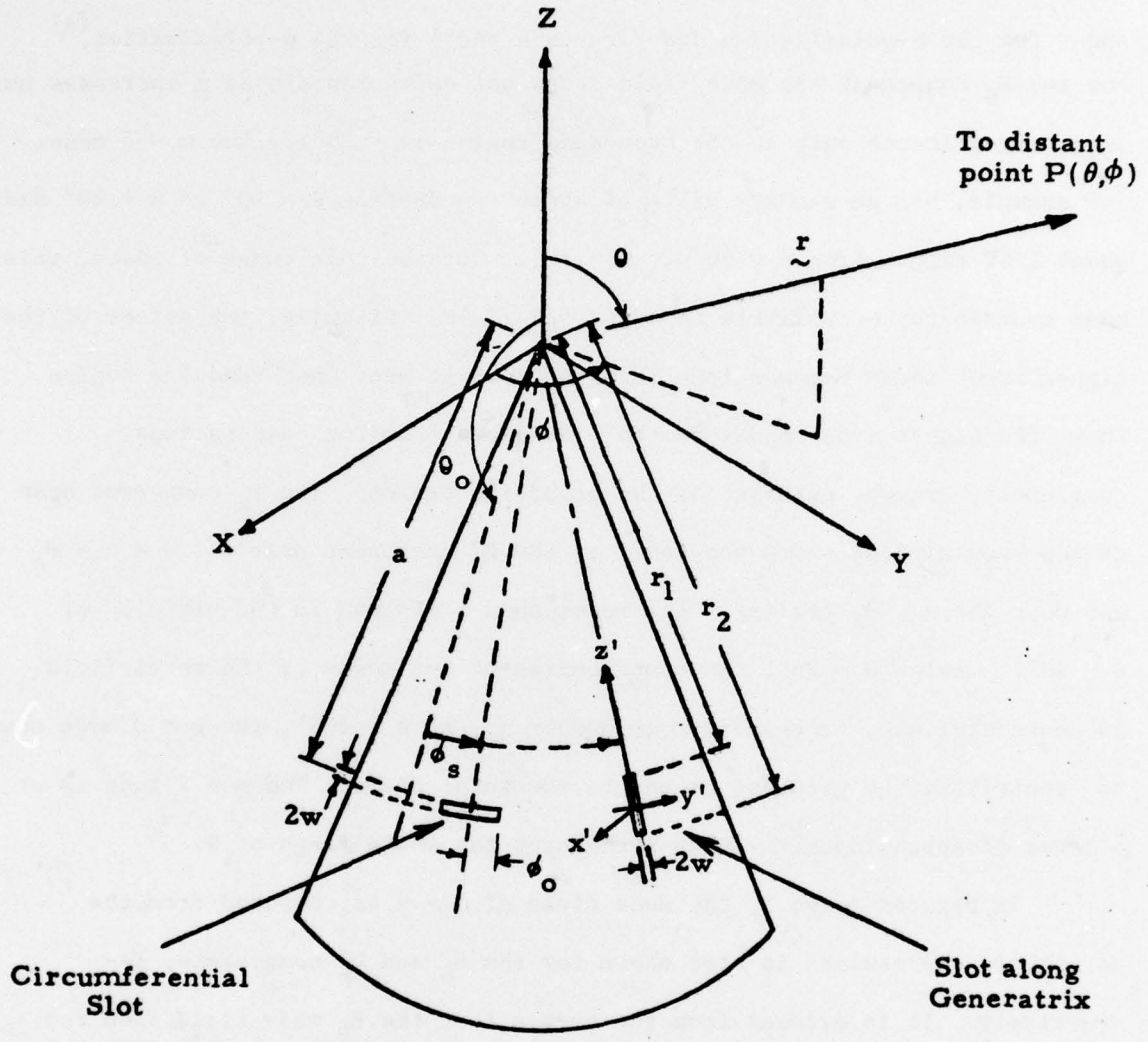

Figure 1. Conical Geometry and Slot Coordinates

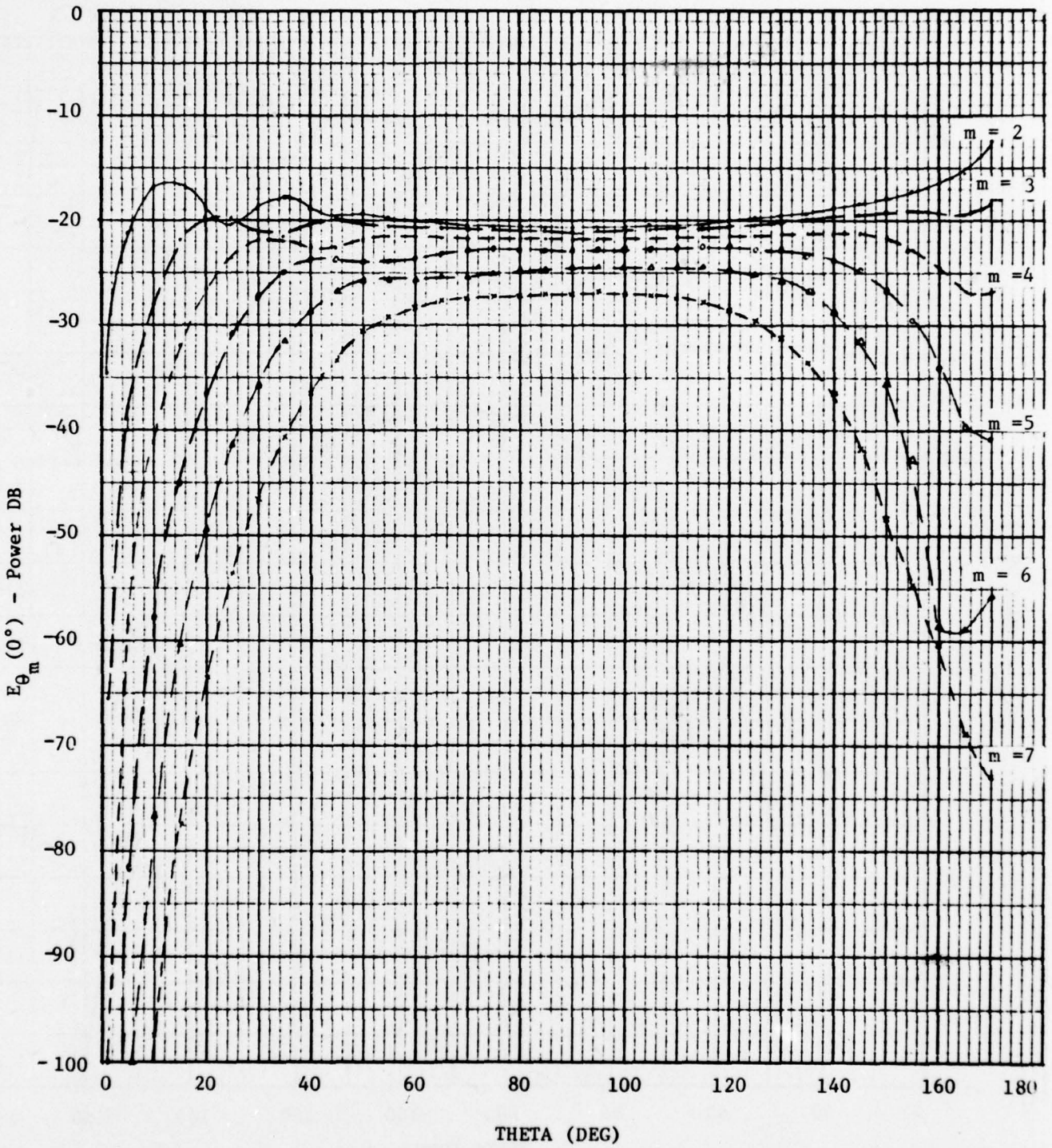

Figure 2. θ-polarized Mode Patterns of a λ/2 Circumferential Slot (Modal Series m=2 to m=7).

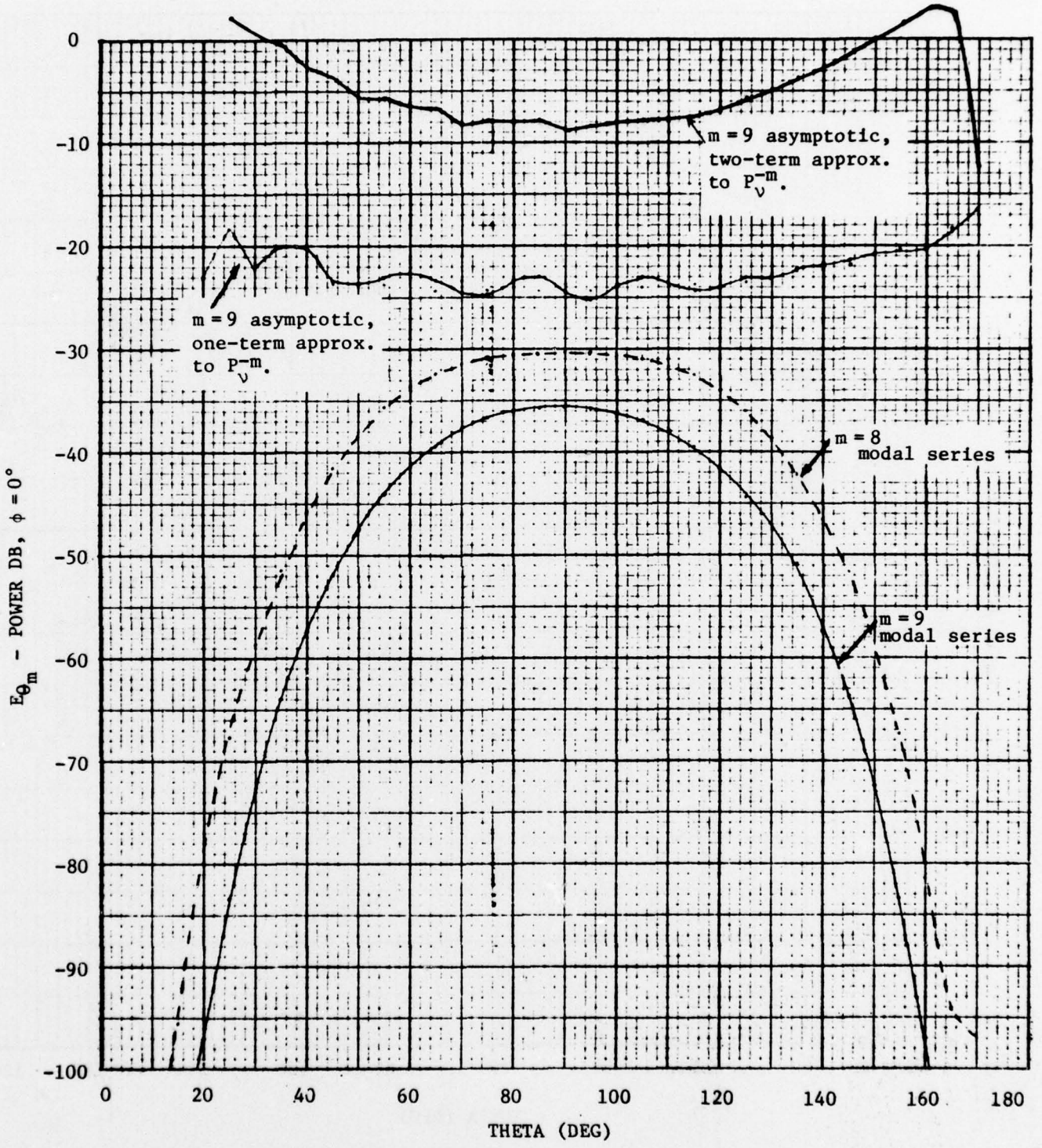

Figure 3. θ-polarized Mode Patterns of λ/2 Circumferential Slot (Modal Series m=8, m=9) and Asymptotic Solutions m=9.

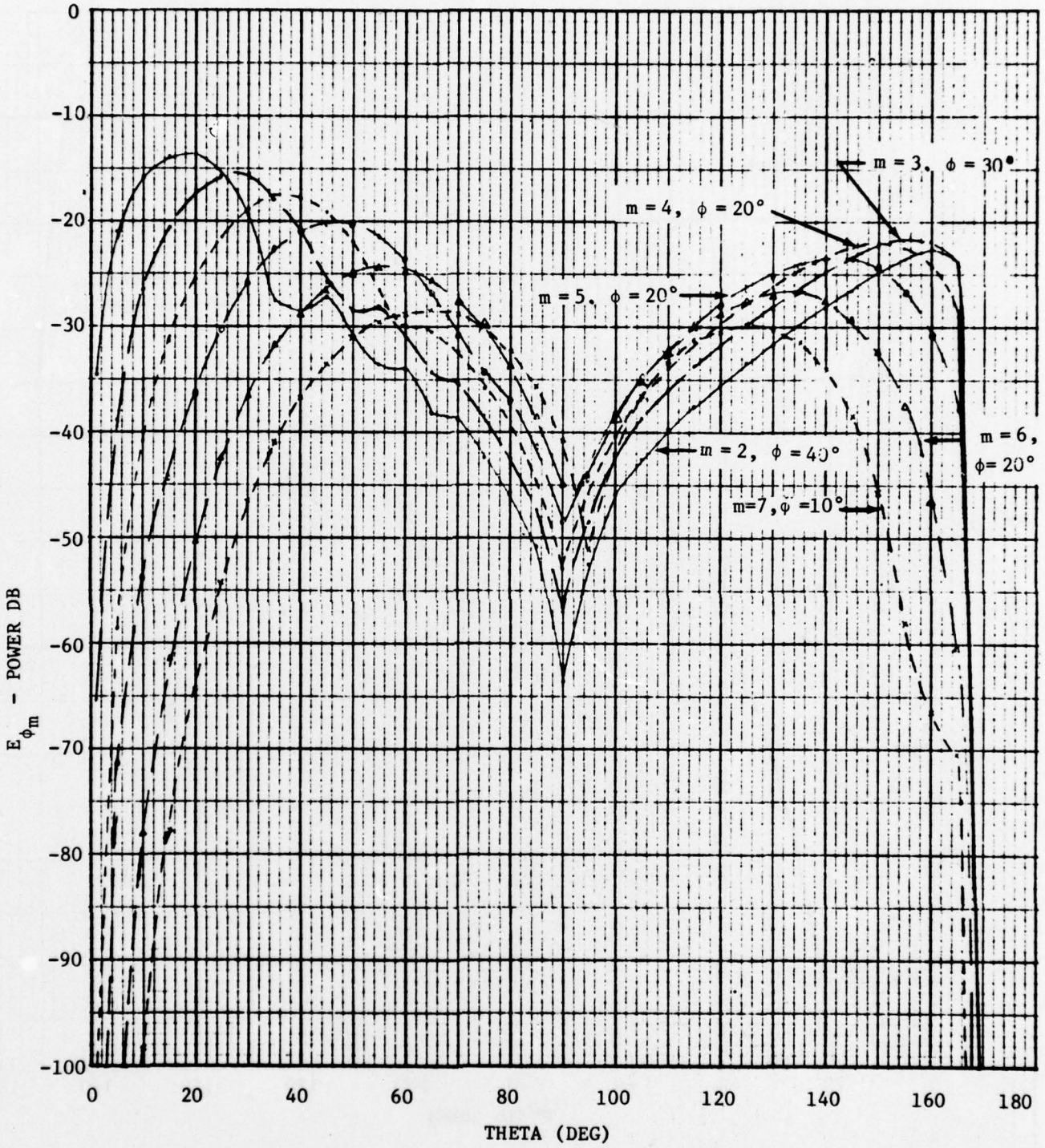

Figure 4. ϕ-polarized Mode Patterns of λ/2 Circumferential Slot (Modal Series m=2 to m=7).

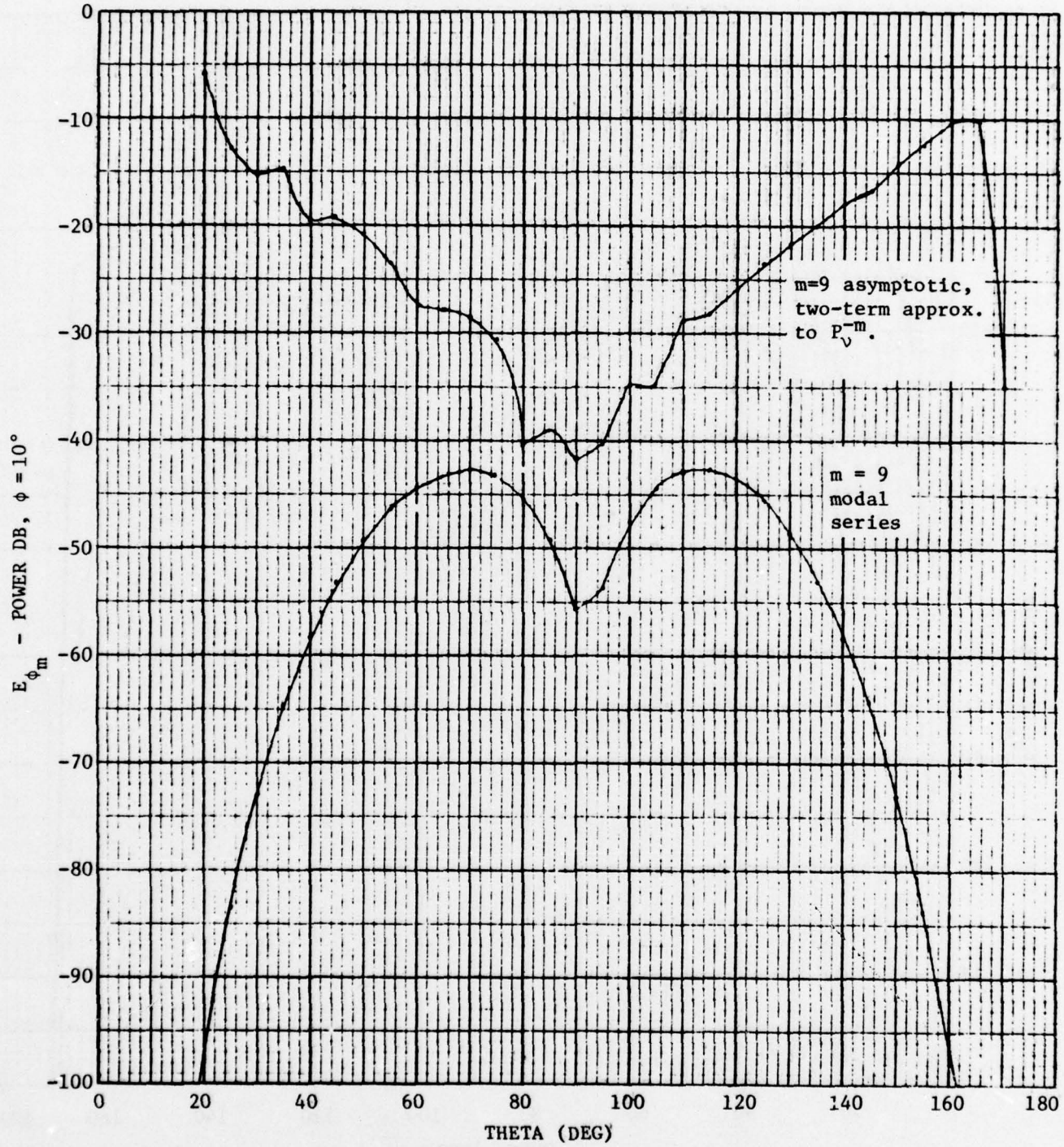

Figure 5. ϕ-polarized Mode Patterns of $\lambda/2$ Circumferential Slot (Modal Series and Asymptotic Solutions m=9).

first term in the approximate representation of the Legendre function, but the convergence problem was not improved significantly. The m = 9 mode field was also computed by a direct Cesàro sum of the series in the diffraction coefficients and without the singularities of the zeroth-order and first order transition field functions T(u) and U(u). Again the computed mode field using asymptotic expressions did not approach the field obtained from the normal mode series.

2.2 Application of Equivalence Principle

A computer program is presently being written to obtain approximate radiation patterns from slot arrays on cones using the equivalence principle. This program is a modification of a Basic language program developed previously (Kummer, et al., 1973). It will use an improved approximation for the slot patterns, similar to that used in the computation of the array patterns presented in this report. The reference patterns that will be approximated in the application of the equivalence principle will be those of a planar array that would fit within the cone. This choice of reference pattern insures that the conformal surface is sufficiently large to be capable of providing a good approximation to the reference pattern. The difference between the synthesized pattern and the reference pattern should then result mainly from the discreteness of the excitation on the cone and from the use of approximate slot patterns. If exact patterns of the slot were used the pattern difference would be essentially due to the discreteness of the excitation.

The program will be capable of orienting the reference pattern in any direction from the tip direction to normal to the tip direction and of

adjusting the polarization at any angle from vertical to horizontal. Thus, the capability of the conformal array to steer a beam of fixed beamwidth will be demonstrated and at the same time excitations required to provide such operation will be determined.

2.3 Quantization Effects on Conical Array Performance:

The conical array computer program that has been used previously to compute patterns from several slot configurations on cones has been modified to simulate the use of digital phase-shifters and digital polarization-rotators.* In its original form of the program, the polarization of each element was rotated in such a way that no cross-polarized energy was radiated by any element in the direction of the peak of the beam. This condition, of course, can in general be met at only one point in the far-field patterns, and cross-polarized energy will exist elsewhere. Even satisfying the condition at the peak of the beam in a practical antenna using crossed slot (or equivalent) elements requires the use of a continuously adjustable variable power divider between the two orthogonal parts of each element.

The phase shifters, as well as the polarization rotators, will be digital devices in conical array systems. Modifications made in the program allow quantization at any number of bits desired in either the phase shift or the polarization rotation. With these modifications a series of patterns has been computed. In most of the computed patterns, 4-bit devices have

---

* The listing of the program and an explanation of many of its parameters may be found in Appendix A of the Jan 1, to April 1, 1973 Quarterly Report, "Dynamic Impedance Matching in Conformal Arrays", Contract N00019-73-C-0127. The Final Report, "Conformal Antenna Arrays Study", Contract N00019-72-C-0212, January 1972 to January 1973, has a compilation of many of the computed patterns.

been assumed for each function; however, some of the results indicate that 3 bits may be adequate for the phase shifter. In a composite digital phase-shifter/polarization-rotator described in the Appendix, two 3-bit digital phase shifters in a parallel arrangement produce both the effects of a 4-bit digital polarization-rotator and a 3-bit digital phase-shifter. The patterns resulting from the use of this device have not yet been simulated in the computer program.

The element configuration used for computing this series of patterns had a total of 432 crossed slots. Their phase centers were arranged in a staggered fashion similar to that shown in Figure 6 with the exception that 48 generatrices were used instead of 32 to bring the elements closer together in the circumferential plane. The generatrices in the 432 element configuration are spaced 7.5° apart in ϕ starting at 3.75°.

It is apparent from Figure 6 that if the beam is pointed in a direction in ϕ that is coincident with one of the generatrices that the elements will tend to be symmetrically disposed in relation to the beam pointing direction. Symmetry also tends to hold if the beam is pointed half-way between two generatrices, although to a lesser degree. Calculations to observe the effects of polarization-rotation quantization showed that these symmetries tended to mask the expected degradations in pattern characteristics. In an effort to avoid the symmetries, and to calculate the worst case, beam pointing directions in ϕ were chosen that differed from the angles of the generatrices by 1/4 of the angular separation between generatrices. Four such angles were determined and used for computing a series of patterns. The angles were ϕ_o^* = 5.625°, 9.375°, 13.125°, and 16.875°, and encompass a variety of asymmetries that should include the worst case.

* In this section θ_o, ϕ_o, refer to the beam pointing directions.

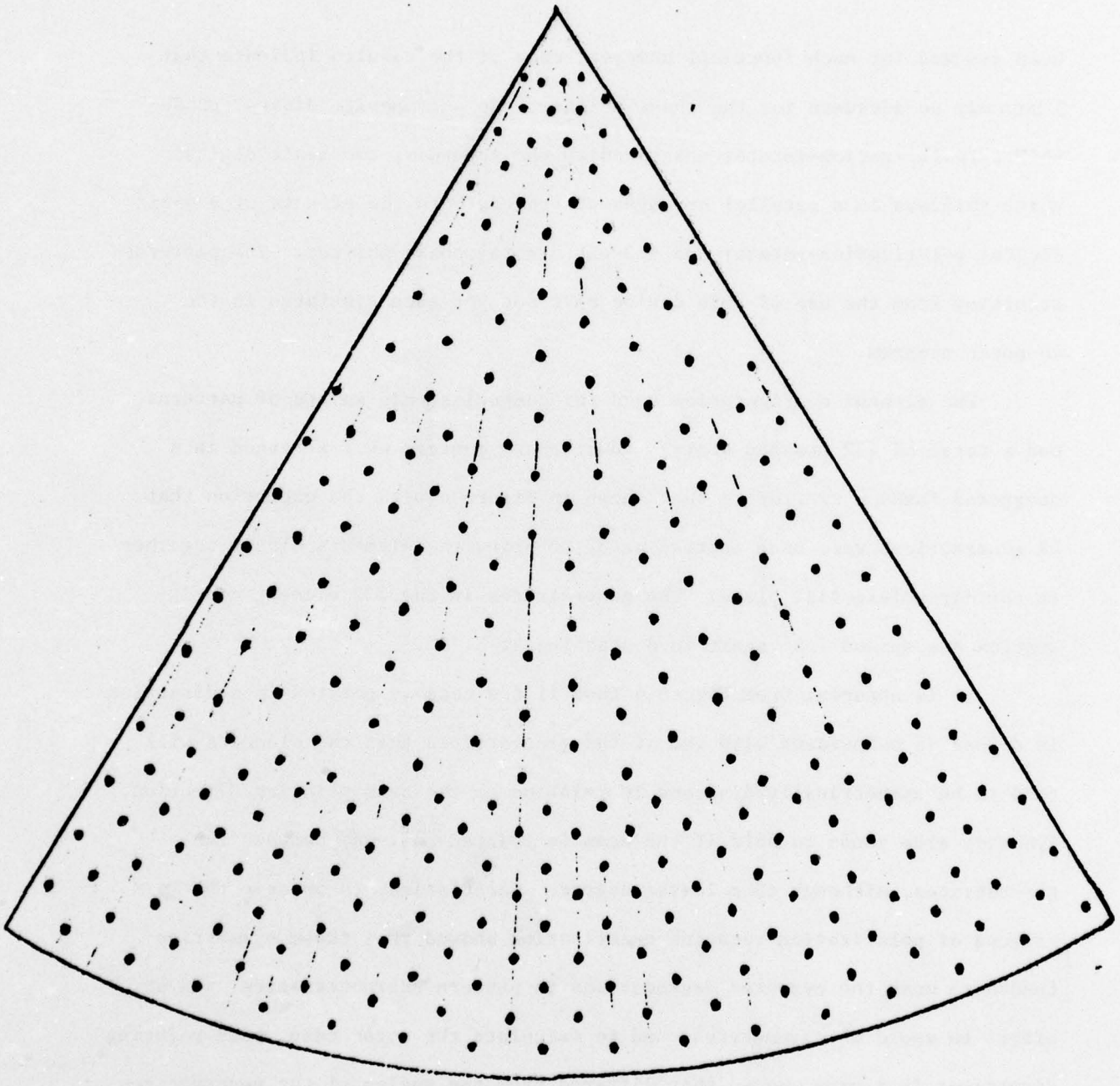

Figure 6.
Scale Drawing of Centers of Phase of the Elements on the Cone in an "Unrolled" View for 288 Element Configuration

A scan angle of $\theta_o = 31.0°$ was chosen as being a typically difficult beam pointing direction for the conical array. θ_o* was held at this value for each of the four scan angles in ϕ mentioned above. For each beam pointing direction in ϕ a series of 8 patterns was computed. Four of these were ϕ cuts (ϕ = constant) for a θ polarized array and produce difference patterns in the longitudinal plane. Four of them were τ cuts with $\tau = 90^o$ for a ϕ polarized array produce difference patterns in the circumferential plane. (See Figure 17). Of the four patterns for each cut, one was a reference pattern with neither polarization-rotation nor phase quantization, one had 4-bit polarization-rotation quantization only, one had 4-bit phase quantization only and the last one had both 4-bit polarization-rotation and 4-bit phase quantization.

The results of these patterns are summarized in Tables I through IV. In the tables four quantities are recorded for each pattern, (1) the sum pattern nominal gain (the values given are relative gains only and are not intended to give an accurate estimate of array gain), (2) sum pattern lst side-lobe level (or shoulder, in some cases), (3) sum pattern cross-polarized component (this is the highest value attained anywhere throughout the pattern and is given in dB below the peak of the sum pattern), (4) the difference pattern null depth (also in relation to the peak of the sum pattern).

A survey of the results shows that quantization effects are not severe, especially with regard to the degradation of the null-depth of the difference patterns. The null depths are consistently lower for the ϕ cuts than for the τ cuts for reasons that are not clear. Computer round-off error as well as

---

* In this section θ_o, ϕ_o, refer to the beam pointing directions.

the different principal polarizations of the two cuts may be factors. The computer program needs to be further modified so that it will compute difference patterns in both principal planes for either θ polarized or ϕ polarized arrays.

The tables show that phase quantization at 4 bits has very little effect on the patterns. It shows up mostly on the 1st sidelobe level, and in the cross-polarized component. It appears that 3-bit phase shifters may be adequate for this array with its relatively large number of elements.

A complete set of patterns for the $\phi_o = 9.375^o$ beam pointing direction is given as being representative of the 4 sets. They are presented in Figures 18 through 33 at the end of the Appendix. A study of these patterns indicates that degradation due to quantization of the polarization-rotation and phase shift is not severe.

Table I. Effect of Quantization of Polarization Rotation and Phase Shift on Conical Array Performance:

Cone Half-Angle = 10.0°

Total No. of Slots = 432

Beam Point Direction: Theta = 31.0° Phi = 5.625°

PATTERN CUT	PRINCIPAL POLARIZATION	PARAMETER	NO QUANTIZATION	POLARIZATION ROTATION QUANTIZED: 4-BITS	PHASE QUANTIZED: 4-BITS	BOTH POLARIZATION ROT. AND PHASE QUANTIZED: 4-BIT
$\phi = 5.625^{\circ}$	θ	Sum Pattern Nominal Gain	15.98dB	15.95dB	15.98dB	15.95dB
		Sum Pattern 1st. Sidelobe	-11.06dB	-11.06dB	-10.91dB	-10.90dB
		Sum Pattern Cross-Pol. Comp.	-43.84dB	-30.20dB	-38.49dB	-28.77dB
		Difference Pattern Null Depth	-57.59dB	-59.73dB	-57.59dB	-59.73dB
$\tau = 90^{\circ}$	ϕ	Sum Pattern Nominal Gain	16.65dB	16.50dB	16.67dB	16.59dB
		Sum Pattern 1st. Sidelobe	-9.41dB	-9.31dB	-8.76dB	-8.76dB
		Sum Pattern Cross-Pol. Comp.	-14.46dB	-13.87dB	-13.85dB	-13.56dB
		Difference Pattern Null Depth	-33.61dB	-37.91dB	-31.70dB	-26.03dB

Table II. Effect of Quantization of Polarization Rotation and Phase Shift on Conical Array Performance:

Cone Half-Angle = 10.0^{o}

Total No. of Slots = 432

Beam Point Direction: Theta = 31.0^{o} Phi = 9.375^{o}

PATTERN CUT	PRINCIPAL POLARIZATION	PARAMETER	NO QUANTIZATION	POLARIZATION ROTATION QUANTIZED: 4-BITS	PHASE QUANTIZED: 4-BITS	BOTH POLARIZATION ROT. AND PHASE QUANTIZED: 4-BIT
$\phi=9.375^{o}$	θ	Sum Pattern Nominal Gain	15.98dB	15.95dB	15.98dB	15.95dB
		Sum Pattern 1st. Sidelobe	-11.06dB	-11.05dB	-11.29dB	-11.24dB
		Sum Pattern Cross-Pol. Comp.	-35.41dB	-30.07dB	-34.47dB	-28.63
		Difference Pattern Null Depth	-73.86dB	-50.41dB	-73.86dB	-50.41dB
$\tau=90^{o}$	ϕ	Sum Pattern Nominal Gain	16.47dB	16.35dB	16.47dB	16.35
		Sum Pattern 1st. Sidelobe	-9.63dB	-9.69dB	-9.04dB	-9.13dB
		Sum Pattern Cross-Pol. Comp.	-16.74dB	-16.98dB	-16.46dB	-16.78dB
		Difference Pattern Null Depth	-35.06dB	-31.49dB	-35.06dB	-31.49dB

Table III. Effect of Quantization of Polarization Rotation and Phase Shift on Conical Array Performance:

Cone Half-Angle = 10.0^{o}

Total No. of Slots = 432

Beam Point Direction: Theta = 31.0^{o} Phi = 13.125^{o}

PATTERN CUT	PRINCIPAL POLARIZATION	PARAMETER	NO QUANTIZATION	POLARIZATION ROTATION QUANTIZED: 4-BITS	PHASE QUANTIZED: 4-BITS	BOTH POLARIZATION ROT. AND PHASE QUANTIZED: 4-BIT
$\phi = 13.125^{o}$	θ	Sum Pattern Nominal Gain	15.98dB	15.90dB	15.98dB	15.90dB
		Sum Pattern 1st. Sidelobe	-11.05dB	-11.04dB	-11.33dB	-11.35dB
		Sum Pattern Cross-Pol. Comp.	-36.05dB	-26.87dB	-33.59dB	-26.87dB
		Difference Pattern Null Depth	-62.52dB	-53.20dB	-62.52dB	-53.20
$\tau = 90^{o}$	ϕ	Sum Pattern Nominal Gain	16.37dB	16.29dB	16.37dB	16.29dB
		Sum Pattern 1st. Sidelobe	-9.96dB	-9.98dB	-9.37dB	-9.41dB
		Sum Pattern Cross-Pol. Comp.	-16.77dB	-16.03dB	-16.34dB	-15.63dB
		Difference Pattern Null Depth	-49.26dB	-45.59dB	-49.26dB	-45.59dB

Table IV. Effect of Quantization of Polarization Rotation and Phase Shift on Conical Array Performance:

Cone Half-Angle = 10.0°

Total No. of Slots = 432

Beam Point Direction: Theta = 31.0° Phi = 16.875°

PATTERN CUT	PRINCIPAL POLARIZATION	PARAMETER	NO QUANTIZATION	POLARIZATION ROTATION QUANTIZED: 4-BITS	PHASE QUANTIZED: 4-BITS	BOTH POLARIZATION ROT. AND PHASE QUANTIZED: 4-BIT
ϕ=16.875	θ	Sum Pattern Nominal Gain	15.98dB	15.91dB	15.98dB	15.91dB
		Sum Pattern 1st. Sidelobe	-11.05dB	-11.05dB	-11.11dB	-11.12dB
		Sum Pattern Cross-Pol. Comp.	-35.84dB	-32.56dB	-32.26dB	-29.37dB
		Difference Pattern Null Depth	-68.66dB	-54.52dB	-68.66dB	-54.52dB
τ=90°	ϕ	Sum Pattern Nominal Gain	16.39dB	16.19dB	16.39dB	16.19dB
		Sum Pattern 1st. Sidelobe	-10.00dB	-9.92dB	-9.35dB	-9.54dB
		Sum Pattern Cross-Pol. Comp.	-15.64dB	-15.07dB	-15.26dB	-14.72dB
		Difference Pattern Null Depth	-33.92dB	-32.67dB	-33.92dB	-32.67dB

3.0 MUTUAL COUPLING CALCULATIONS OF NARROW CIRCUMFERENTIAL SLOTS ON A CYLINDER

Expressions for the computation of mutual coupling between circumferential slots on a cylinder have been found in terms of cylindrical harmonics by Golden, et al. The harmonic series results in precise calculation of mutual coupling between two slots on a cylinder and it can be used to check results from approximate asyptotic expressions using the Geometrical Theory of Diffraction. The pertinent geometry of the circumferential slots on the cylinder is shown in Figure 7.

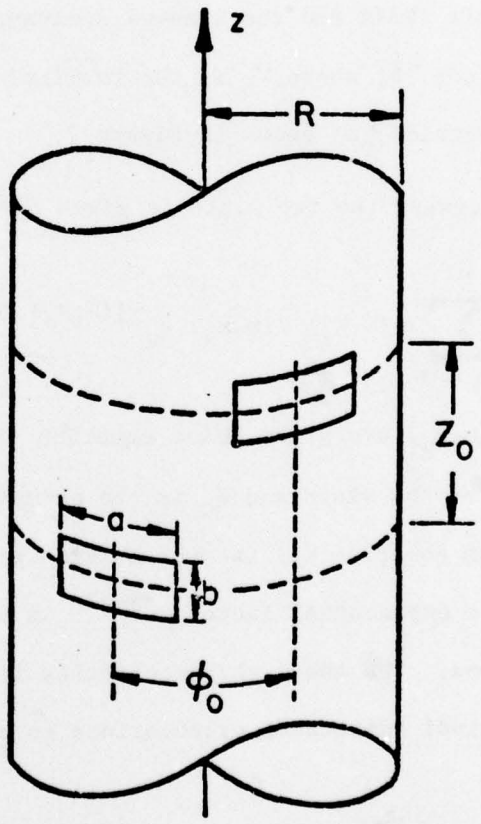

Figure 7. Circumferential Slots on the Surface of a Cylinder.

The harmonic series has been used to calculate self and mutual admittance of circumferential slots on a cylinder. The results of computations for two different types of slots are presented in the following section. In section 3.2, some preliminary results of the behavior of the input admittance of a slot in a planar array environment are presented.

3.1 Mutual Admittance Calculations of Circumferential Slots.

In the harmonic series approach, the stationary formula for self and mutual admittance of two slots is expressed in terms of the Fourier transforms of the surface magnetic field and the assumed dominant mode aperture electric field, $E_z = V_o \sqrt{\frac{2}{ab}} \cos \frac{\pi y}{b}$, where V_o is the terminal voltate and a,b are the dimensions of the waveguide, as shown in Figure 7.

The admittance between the two slots is given by equation (8) of Golden, et al., (1974) as

$$Y_{ij} = \frac{a\,b}{8\pi^2 \rho_o} \int_{-\infty}^{\infty} \sum_{m=-\infty}^{\infty} \psi(m,k_z)\, Y(m,k_z)\, e^{-j(k_z z_o + m\phi_o)}\, dk_z \qquad (1)$$

where $\psi(m,k_z)$, and $Y(m,k_z)$ are given below equation (8). The quantity z_o is the axial separation of the slots and ϕ_o is the azimuthal slot separation. As it can be seen from equation (1) the integration with respect to k_z is of infinite range and the exponential factor $e^{-jk_o z_o}$ is highly oscillatory for large axial separations. The above characteristics limit the usefulness of the expression for mutual admittance calculations to axial slot separations of a few wavelengths.

The computer program describing the harmonic series* has been used to compute mutual admittance of two circumferential slots on the cylinder as a function of axial and azimuthal slot separations for cylinder radii of 1.991", 3.777" and 6.0". The original computer program has been modified in some respects and has been excuted successfully on the Control Data Corporation 7600 computer. Initial computations were made with a $0.69\lambda \times 0.31\lambda$ rectangular slot at 9 GHz.

The programmed expressions have been normalized to the characteristic admittance of the feed waveguide,

$$Y_g = Y_o \sqrt{1 - \left(\frac{\pi}{k_o b}\right)^2} \quad , \text{ where } Y_o = (\varepsilon_o/\mu_o)^{1/2}$$

and k_o is the free space wavenumber. The integration is performed over the normalized independent variable range of $0 \leq k_z/k_o \leq 4$ since the expression for Y_{ij} is an even function of k_z. The sufficiency of the integration range is determined by looking at the self or mutual admittance calculations starting at a specified value of k_z/k_o and noting the change in its value as the integration range is extended incrementally. For the cases considered here, i.e., cylinder radii R = 1.991", R = 3.777" and R = 6.0", the integration range extends to $k_z/k_o = 8.5$ for the last case. The convergence of the harmonic series is similarly checked by noting the change in the admittance as the number of terms in the series is increased for the specified integration range. It was found that approximately 70 terms were required for proper convergence of the harmonic series. For larger cylinders both the integration range and the number of terms in the series may have to be increased.

When $k_z = k_o$, non-integrable singularities are introduced in the expression of $Y(m,k_z)$ of equation (1). Because of these singularities, it is necessary to assume that free space has a small loss tangent.

---

* Original program courtesy of Dr. Gordon Stewart, Aerospace Corporation, El Segundo, California

Variation in this loss tangent produces small changes in Y_{11} which are negligible. For small separations, Y_{12} is unaffected by the loss tangent, but for larger angular and axial separations the loss tangent can affect Y_{12} significantly. Figure 8 shows the effect of the assumed free space loss tangent on the calculated self and mutual admittance for a 6" redius cylinder and axial slot separation of 16 inches.

Table V shows calculated values of self and mutual admittance of slots on a 6" radius cylinder with 16 inches of separation. The integration range is divided into two sub-ranges, k_{z1} and k_{z2} with corresponding step-size Δk_{z1} and Δk_{z2}. In the present calculations k_{z1} has been specified at 1.5 and $\Delta k_{z2} = 5\ \Delta k_{z1}$. As can be seen from the tabulated values, the admittance values are changed significantly when the step size is reduced by 25% for a specific number of modes in the series. The tabulated data also show the effect of the assumed loss tangent of free space.

Mutual admittance values between circumferential slots as a function of axial separation are shown in Figure 9 for the cylinder radii indicated. Phase angle data are tabulated in Table VI. It is evident from the curves from the Stewart-Golden program that the coupling is increasing with increasing curvature.

Calculated values of mutual coupling coefficients for the circumferential slots considered are shown in Table VII together with measured* values for the R = 1.991" case. Measured and calculated values are in very close agreement. It is concluded that the computer program gives accurate results for up to six inches of axial slot separation.

---

* Courtesy of Dr. Gordon Stewart, Aerospace Corporation, El Segundo , California.

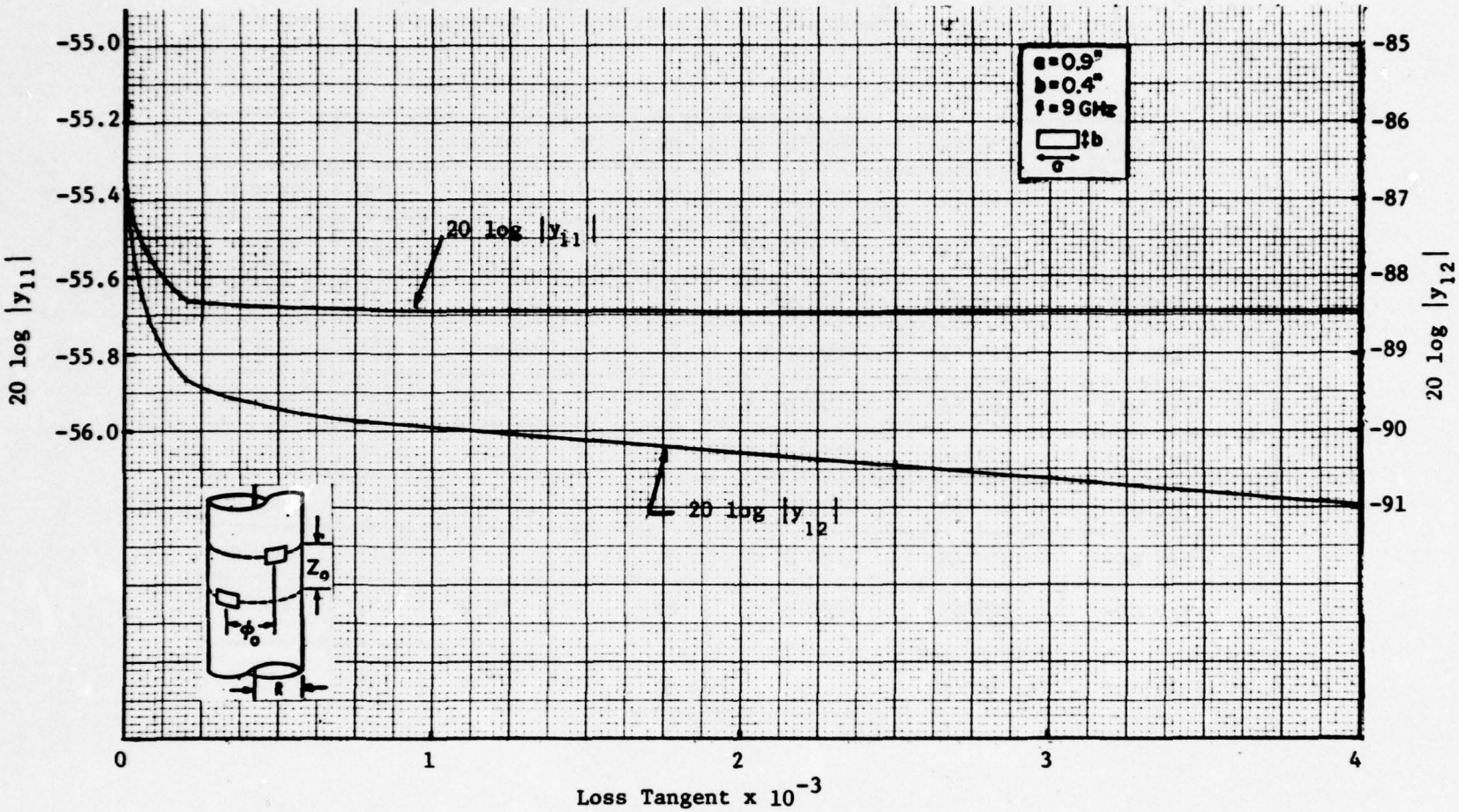

Figure 8. Self and Mutual Admittance as a Function of Assumed Free Space Loss Tangent (R=6", Z_o = 16", ϕ_o = 0°).

Δk_{z1}	k_{z1}	Δk_{z2}	k_{z2}	m	ε	20 log $\lvert Y_{11} \rvert$	20 log $\lvert Y_{12} \rvert$
0.002	1.5	0.01	4	80	1-j0.0025	-55.695	-90.474
0.002	1.5	0.01	4	70	1-j0.0025	-55.676	-90.474
0.0015	1.5	0.0075	4	80	1-j0.0025	-55.694	-90.491
0.0015	1.5	0.0075	8.5	80	1-j0.0025	-55.654	-90.490
0.002	1.5	0.01	4	80	1-j0.00125	-55.692	-90.035
0.0015	1.5	0.0075	8.5	80	1-j0.00125	-55.655	90.094
0.0015	1.5	0.0075	4	70	1-j0.00125	-55.676	90.095
0.0002	1.5	0.01	4	80	1-j0.0002	-55.663	-89.336
0.0002	1.5	0.001	4	80	1-j0.004	-55.695	-90.973
0.002	1.5	0.01	4	80	1-j0.00001	-55.369	-85.798

Table V. Admittance Calculations of Circumferential Slots on a Cylinder for Different Integration Ranges and Loss Tangent (Cylinder Radius = 6", Axial Slot separation = 16", Azimuthal slot separation = 0^{o}).

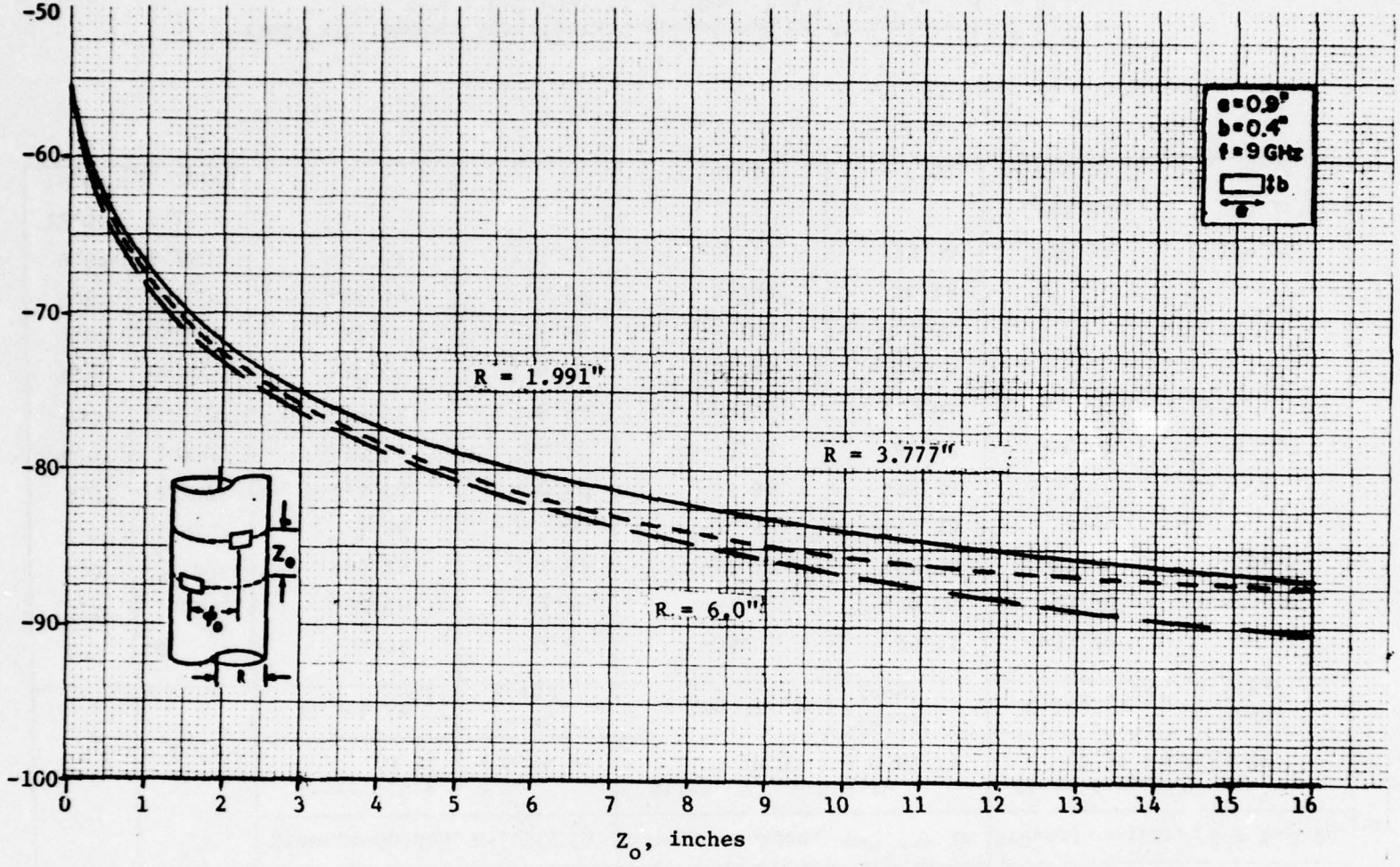

Figure 9. Mutual Admittance of Circumferential Slots, $Y_o = 0°$

Z_o	Z_o/λ	Stewart-Golden, R=1.991 in. Slot: 0.4 x 0.9 in. (0.31 λ x 0.69 λ)		Stewart-Golden, R=3.777 in. Slot: 0.4 x 0.9 in. (0.31 λ x 0.69 λ)		Stewart, Golden, R = 6.0 in. Slot: 0.4 x 0.9 in. (0.31 λ x 0.69 λ)	
		20 log $\lvert Y_{12} \rvert$	Phase (deg)	20 log $\lvert Y_{12} \rvert$	Phase (deg)	20 log $\lvert Y_{12} \rvert$	Phase (deg)
0"	0	-55.35	24.06	-55.62	25.71	-55.70	26.91
0.5"	0.3813	-62.61	72.38	-63.02	-70.06	-63.20	-69.04
1.0"	0.7626	-66.86	154.67	-67.43	158.06	-67.67	159.56
2.0"	1.5252	-71.86	-117.00	-72.68	-112.33		
3.0"	2.2878	-74.96	-30.90	-75.96	-25.39		
4.0"	3.0503	-77.02	54.11	-78.17	60.17	-78.67	63.02
5.0"	3.8129	-78.76	138.54	-80.06	145.06		
6.0"	4.5755	-80.06	-136.10	-81.46	-129.17		
7.0"	5.3381	-81.17	-52.40	-82.68	-45.31		
8.0"	6.1007	-82.30	32.65	-83.94	40.18		
9.0"	6.8633	-83.07	117.61	-84.77	125.36	-85.51	129.24
12.0"	9.1511					-88.04	25.38
16.0"	12.2014			-87.35	- 6.01	-90.47	8.14

Table VI. Mutual Admittance Computations of Circumferential Slots on a Cylinder (f = 9 GHz, λ = 1.3113 in., ϕ_o = 0°).

	20 log $\|S_{12}\|$		20 log $\|S_{12}\|$	
Z_o in.	R=1.991" Calculated	R=1.991" Measured	R=3.777" Calculated	R= 6.0" Calculated
0.5	-13.29	-13.1	-13.36	-13.41
1.0	-17.12	-17.3	-17.36	-17.48
1.5		-20.1		
2.0	-22.18	-22.2	-22.68	
2.5		-23.8		
3.0	-25.26	-25.1	-25.94	
3.5		-26.3		
4.0	-27.31	-27.5	-28.16	-28.53
5.0	-29.06		-30.04	
5.5	-29.71	-29.9		
6	-30.35		-31.44	
7	-31.47		-32.67	
8	-32.59		-33.92	
9	-33.37		-34.75	-35.38
12				-37.90
16	-37.65			-40.34

Table VII. Calculated and Measured Mutual Coupling of Circumferential Slots on a Cylinder at 9 GHz.

The mutual coupling calculations with the $0.69\lambda \times 0.31\lambda$ slot indicated that a stronger coupling exists between two circumferential slots displaced along the Z - axis than between corresponding slots on a planar surface. To further substantiate this phenomenon, additional computations were made using a narrow half-wavelength slot ($0.5\lambda \times 0.01\lambda$) at 9 GHz. The narrow slot was proposed by Hansen (1976), since such a slot is more representative of the type of slots used in many slot arrays.

Additional constraints on the computer program are imposed for this calculation. For example, the narrow slot requires considerably more modes in the harmonic series before convergence of the series is realized. Also, the integration range must be extended. The integration range required was again determined by observing the change in the calculated self admittance or mutual admittance as the integration range was extended incrementally past a specified value of k_z/k_o. Figure 10 shows the effect of the integration range on the self admittance ($Z_o = 0"$, $\phi_o = 0^o$) for the three different cylinder radii considered. Figure 11 shows the mutual admittance as a function of the integration range of two slots on a 3.777" radius cylinder displaced 8" along the Z-axis. The oscillatory behavior of the mutual admittance for large axial displacements of the slots is clearly evident. The self admittance, on the other hand, shows an asymptotic behavior for all three cases considered. As in the previous calculations, free space is assumed to have a small loss tangent ($\tan \delta = 0.0025$)

Mutual admittance computations for the narrow slot were performed with 80 modes in the modal series and minimum acceptable integration range. The consideration of additional harmonic modes and extension of the integration range greatly increase the cost of computation and seemed unwarranted for

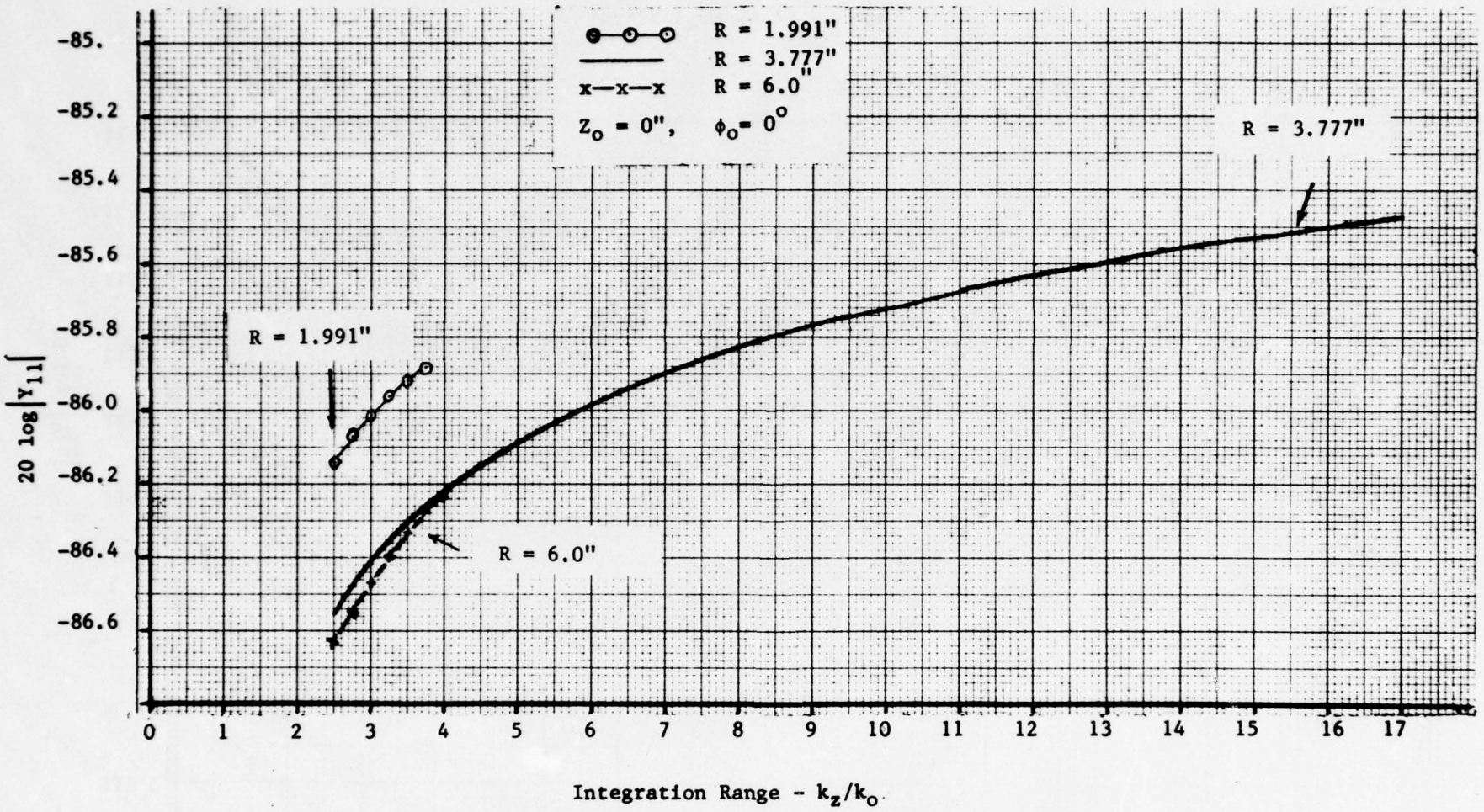

Figure 10. Self Admittance of Narrow Circumferential Slot as a Function of Integration Range.

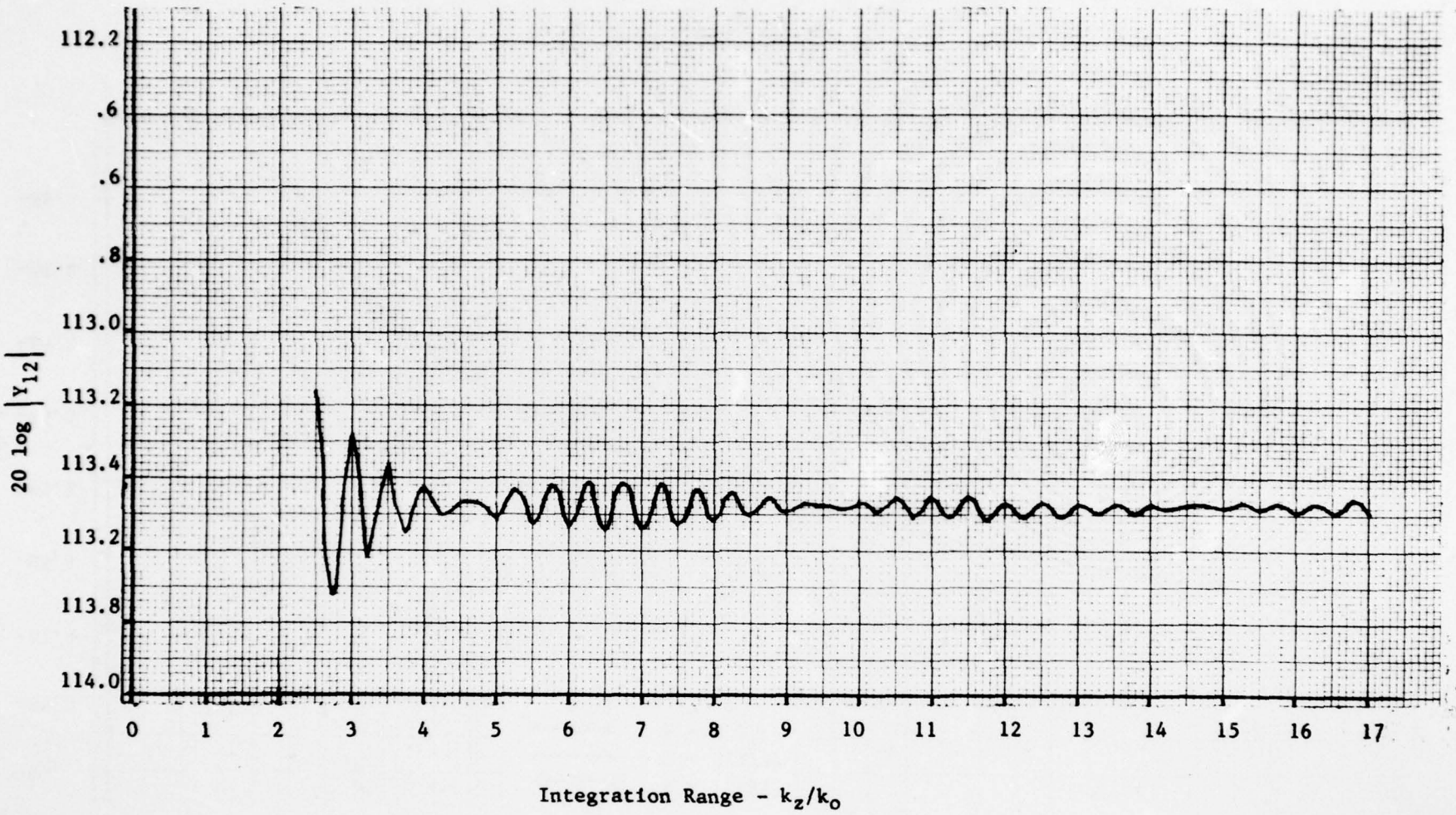

Figure 11 Mutual Admittance of Narrow Circumferential Slot as a Function of Integration Range.

the small improvement in the final result at this time. Figure 12 shows once again the stronger coupling between the axially displaced narrow slots on the cylinder with increased transverse curvature (small radius). This phenomenon has also been confirmed by Lee (1976) using an alternate modal solution and also an asymptotic solution. All mutual admittance results between narrow slots are unnormalized.

Mutual admittance curves for axial separations of 0", 2" and 4" are shown in Figures 13,14, and 15 for cylinder radii of 1.991", 3.777" and 6.0", respectively. In all three cases a stronger coupling is noted for large azimuthal slot separations and large axial separations. This is opposite to what happens for small azimuthal separations. In the vicinity of $\phi = 10°$ and particularly for the $Z_o = 0"$ cases, the calculated values are somewhat higher than expected. This region, however, represents the condition of overlapping slots and is not a practical case. For the cases considered, the overlapping regions occur when $\phi_o \leq 18.88°$ for R = 1.991", $\phi_o \leq 9.95°$ for R=3.777" and $\phi_o = 6.26°$ for R = 6.0".

The phase information of the mutual admittance, calculations for the different cases considered is tabulated in Tables VIII and IX.

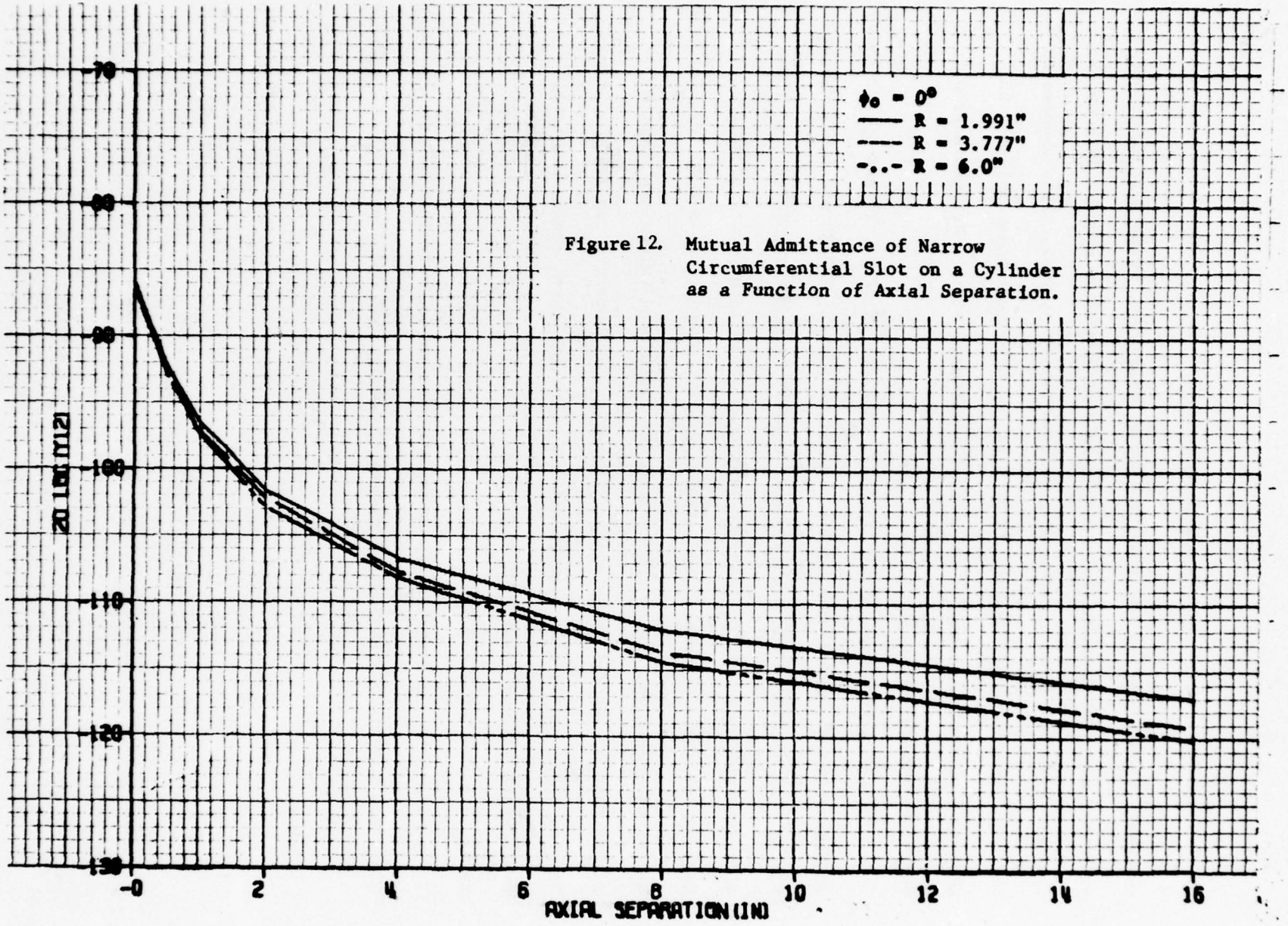

Figure 12. Mutual Admittance of Narrow Circumferential Slot on a Cylinder as a Function of Axial Separation.

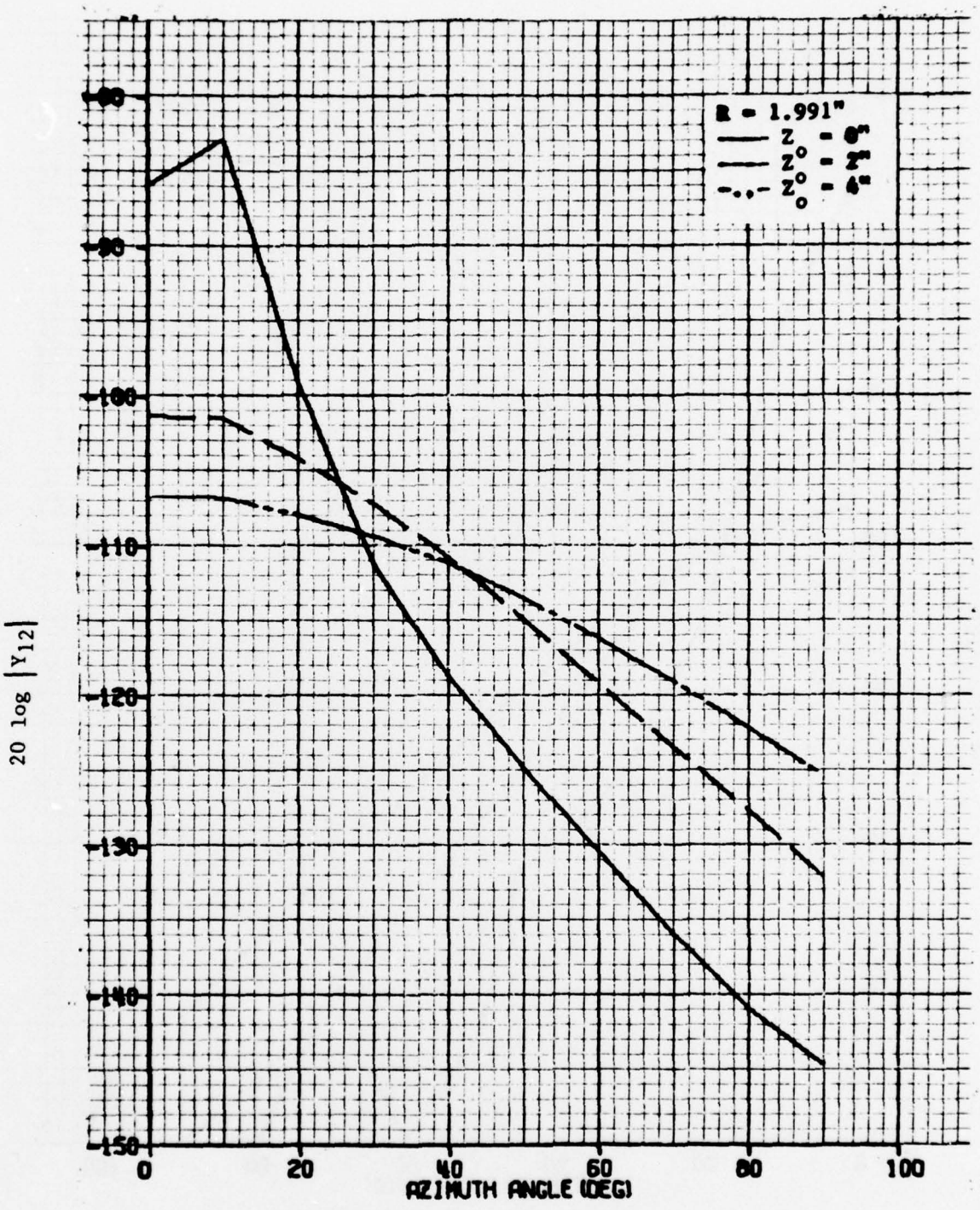

Figure 13. Mutual Admittance of Narrow Circumferential Slot as a Function of Azimuthal Slot Separation

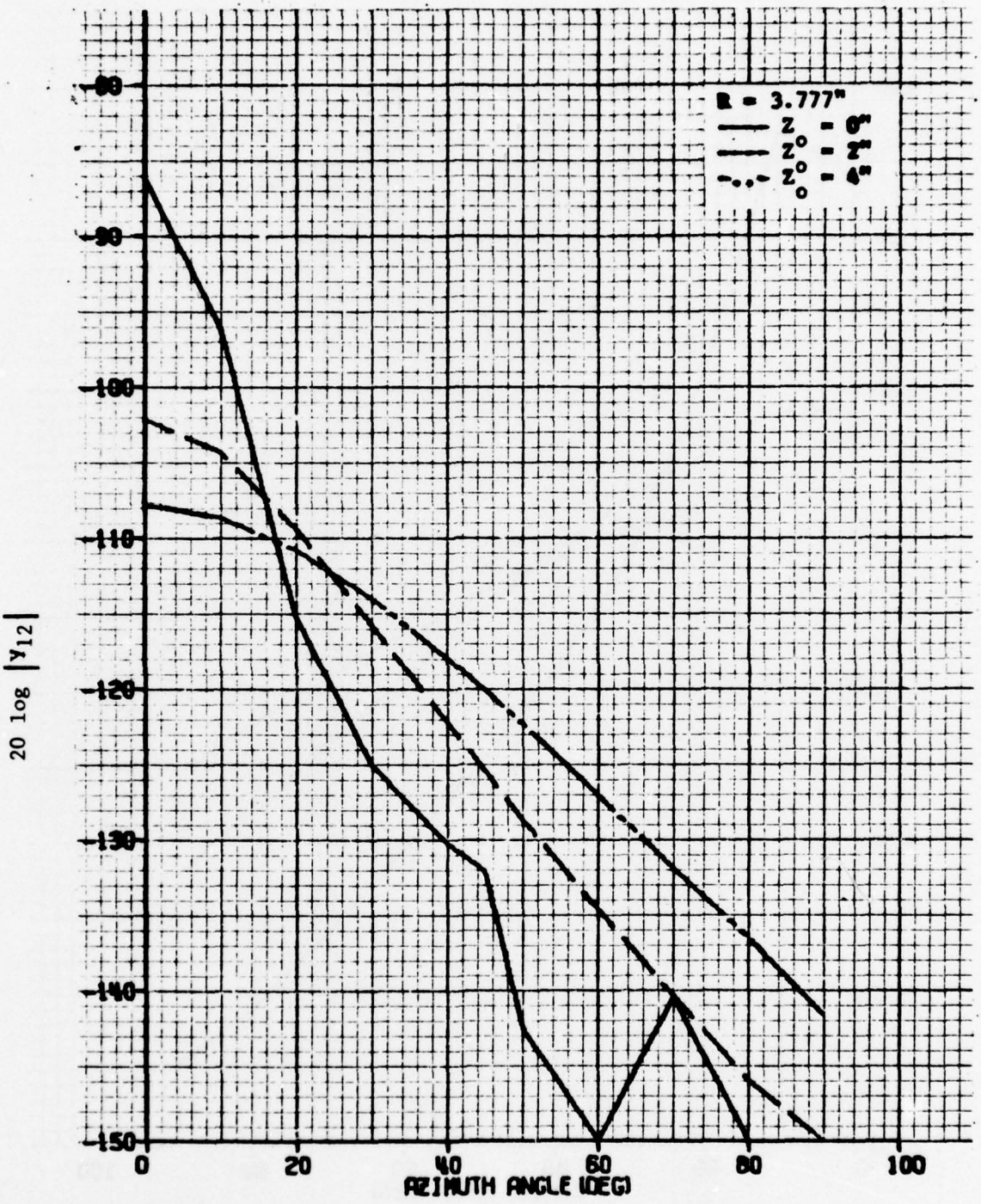

Figure 14. Mutual Admittance of Narrow Circumferential Slot as a Function of Azimuthal Slot Separation.

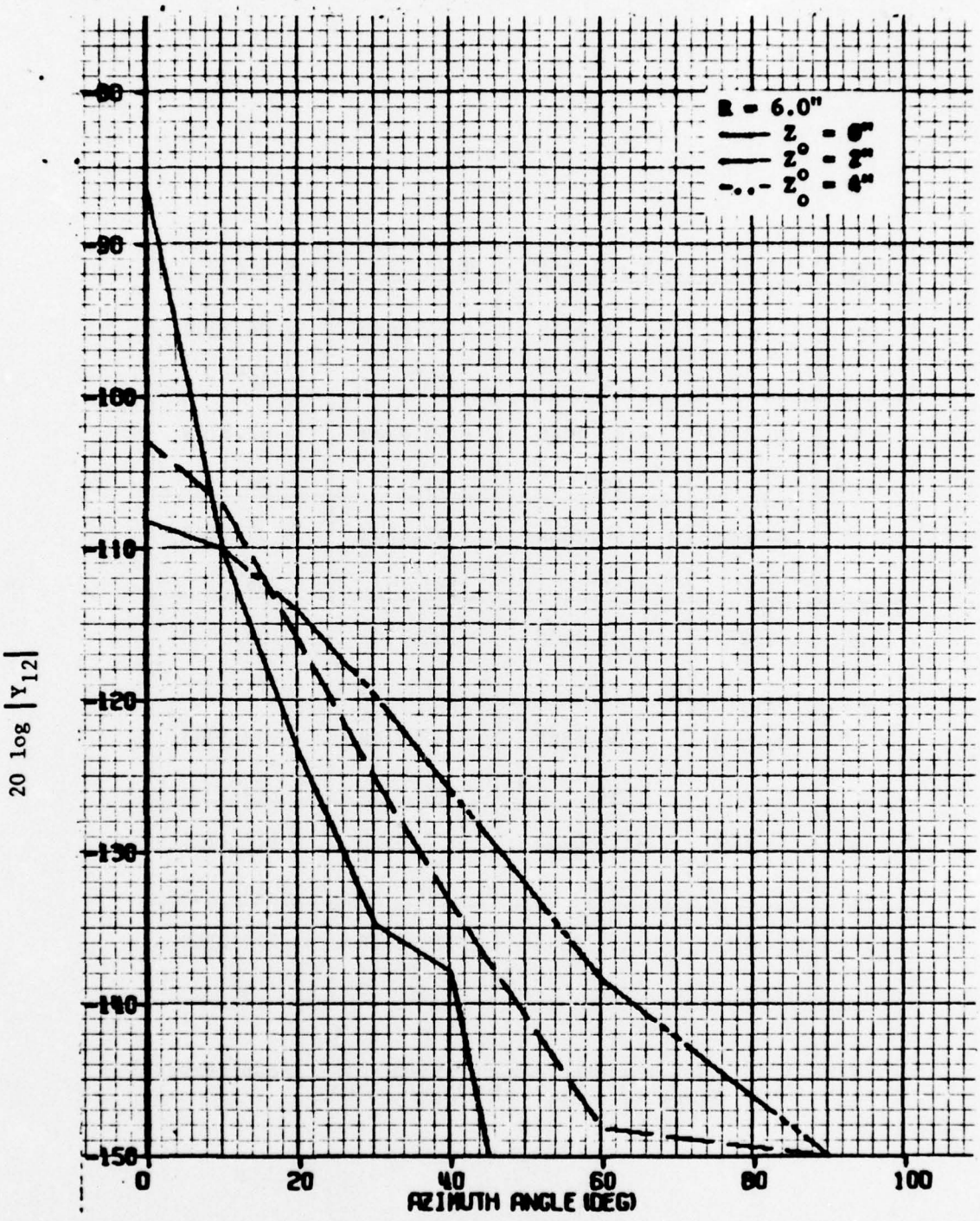

Figure 15. Mutual Admittance of Narrow Circumferential Slot as a Function of Azimuthal Slot Separation.

Z_o	Z_o/λ	R = 1.991"	R =3.777"	R = 6.0"
0"	0	- 85.89dB 24^o	- 86.26dB 26^o	- 86.23dB 29^o
.5"	0. 3813	- 92.30dB -79^o	- 92.83dB -77^o	- 92.87dB -76^o
1"	0.7626	- 96.53dB 154^o	- 97.18dB 157^o	- 97.34dB 156^o
2"	1.5252	-101.33dB 117^o	-102.17dB 113^o	-102.90dB -112^o
4"	3.0503	-106.65dB 54^o	-141.71dB -145^o	-108.19dB 63^o
8"	6.1007	-112.02dB 33^o	-113.65dB 40^o	-114.42dB 44^o
16"	12.2014	-117.08dB -6^o	-119.27dB 3^o	-120.22dB 9^o

Table VIII. Mutual admittance of .5λ x .01λ Circumferential Slots on a Cylinder for $\phi_o = 0^o$.

ϕ_o	R = 1.991"			R = 3.777"			R = 6.0"		
	Z_o = 0"	Z_o = 2"	Z_o = 4"	Z_o = 0"	Z_o = 2"	Z_o = 4"	Z_o = 0"	Z_o = 2"	Z_o = 4"
0°	- 85.89dB 24°	-101.33dB -117°	-106.65dB 54°	- 86.26dB 26°	-102.17dB -113°	-107.83dB 60°	- 86.23dB 29°	-102.90dB -112°	-108.16dB 63°
10°	- 82.85dB 62°	-101.41Db -123°	-106.76dB 51°	- 96.07dB 29°	-104.29dB -140°	-108.66dB 44°	-110.06dB -100°	-107.08dB -178°	-110.02dB 24°
20°	- 99.02dB 11°	-104.11dB -150°	-107.90dB 35°	-115.32dB -176°	-109.38dB 142°	-110.80dB - 2°	-123.36dB - 53°	-116.02dB 10°	-114.12dB - 84°
30°	-111.20dB -106°	-107.07dB 172°	-109.31dB 12°	-125.06dB - 20°	-115.74dB 26°	-114.00dB - 76°	-134.72dB 4°	-125.09dB 139°	-119.66dB 113°
40°	-118.74dB 43°	-110.73dB 121°	-111.18dB -20°	-130.29dB -128°	-122.21dB -115°	-117.96dB -172°	-137.75dB - 77°	-133.24dB -121°	-125.86dB - 89°
45°	-121.68dB 91°	-112.73dB 91°	-112.28dB - 38°	-132.13dB 65°	-125.43dB 168°	-120.11dB 132°	-155.35dB 64°	-137.17dB 104°	-128.98dB 158°
50°	-124.80dB 39°	-114.82dB 59°	-113.47dB - 11°	-142.61dB 88°	-128.68dB 73°	-122.34dB			
60°	-130.40dB - 68°	-119.10dB - 12°	-116.12dB -105°	-151.05dB 144°	-134.62dB 80°	-127.06dB - 57°	-154.06dB -131°	-148.15dB - 43°	-138.39dB 154°
70°	-135.90dB -167°	-123.38dB - 90°	-119.04dB -158	-140.50dB - 84°	-140.33dB 110°	-131.92dB 161°			
80°	-140.95dB 76°	-127.61dB -171°	-122.12dB 143°	-160.99dB - 85°	- 45.95dB - 72°	-136.53dB 12°			
90°	144.60 dB - 8°	-132.06dB 105°	-125.29dB 79°	-150.50dB 86.54	-151.45dB 118°	-141.71dB -145°	-152.79dB 81°	-164.67dB -115°	-155.28dB 71°

TABLE IX. Mutual Admittance (Y_{12}) of .5λ x .01λ Circumferential Slot on a Cylinder

3.2 Active Admittance of Planar Array Elements.

In order to be able to select the most appropriate method of computation for a given configuration, it is desirable to know what effect the accuracy of computation or measurement of the mutual coupling has on the active admittance since mutual coupling of slots on a cylinder can be calculated by various approximate methods. Some methods result in more exact calculations than others; also the degree of complexity in the numerical computations varies with the method selected.

A planar array computer model of half height X-band waveguide slots was selected for the admittance calculations. It was felt that the result obtained for the planar case would indicate the accuracies required for the cylindrical case. Mutual coupling coefficients of a 20 x 40 element array were computed by an existing planar array computer program assuming dominant mode incidence on the aperture. The program utilizes mode matching techniques at the waveguide aperture; ten waveguide modes and forty-five space modes were assumed in the calculation. A triangular lattice configuration as shown in Figure 16 was selected for the model.

The admittance matrix, [Y], may be determined from

$$[Y] = \Big[[U] - [S] \Big] \Big[[U] - [S] \Big]^{-1} \qquad (2)$$

where [S] is the scattering matrix defined by the mutual coupling coefficients and [U] is the identity matrix. Conversly, the scattering matrix may be found from the admittance matrix from the expression

$$[S] = \Big[[U] + [Y] \Big]^{-1} \Big[[U] - [Y] \Big] \qquad (3)$$

Once the admittance matrix is determined from equation (2), the active admittance of the ith element of the array is given by

$$Y_{i\ \text{active}} = \sum_{j=1}^{N} Y_{ij} \qquad (4)$$

The effect of the accuracy of computation of the Y_{ij}s on the active admittance may be evaluated by introducing a small random variation (magnitude and phase) on the Y_{ij}s of equation (4).

Some preliminary calculations were made with a 19-element array in the configuration shown in Figure 16. The active admittance of the center element of the array was calculated after introducing three, five and ten percent maximum random variation in the magnitude and phase variations from 0° to 20° in each of the elements of the admittance matrix.

Preliminary computations indicated that the size of the array chosen may have been too small to obtain meaningful results.

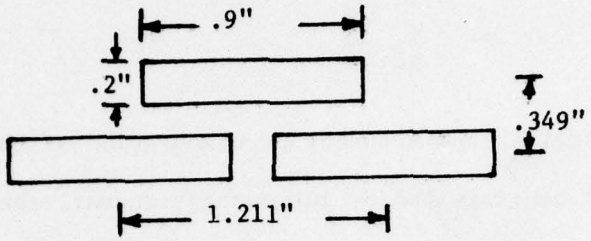

a) array slot dimensions

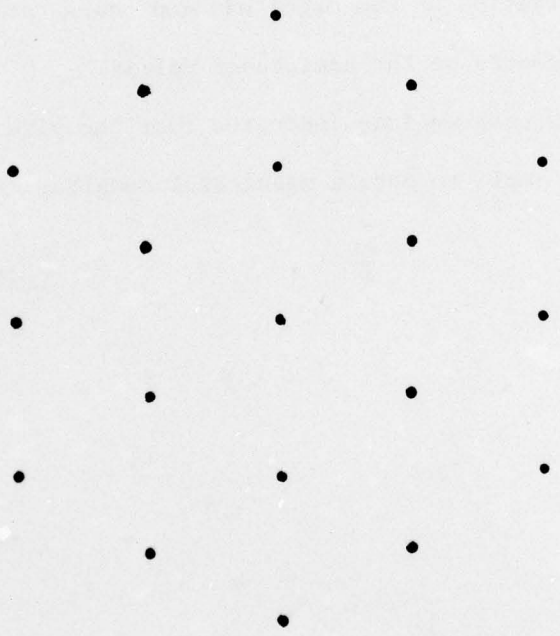

b) 19 - element array configuration

Figure 16. Slot Configuration of Assumed Planar Array Model

4.0 RECOMMENDATIONS FOR FURTHER INVESTIGATIONS

Radiation patterns of arrays on conical or other more generally curved surfaces may be computed by application of the equivalence principle technique. The eqivalence principle technique allows the pattern synthesis to be carried out by using a convenient reference source located within the curved surface and by determining the fields of the reference source over that surface; from these fields the equivalent sources on the surface can be determined. The application of the technique, however, will require the development of a computer program with an improved element pattern. The modal series solution can be used to check the accuracy of the equivalence principle technique.

In addition, another computer program which calculates sum and difference patterns of a conical array has been modified to take into account quantization effects. Although this program uses simple approximations to the element patterns of the slots on the cone and does not take into account mutual coupling, it can calculate difference patterns and can be used to obtain a measure of the sensitivity of the null depth when the following three parameters are quantized: 1) polarization rotation, 2) phase, and 3) amplitude. In an actual array it is very likely that these parameters will be varied by digital hardware devices. The preliminary results of the program using quantized parameters are encouraging. Additional computations, however, are necessary for an accurate assesment of the sensitivity of the null on the quantization of the above three parameters.

During the period of this contract the problem of mutual coupling between slots on a cylinder was also addressed in great detail. However, additional mutual coupling computations on cylindrical structures should be performed for various slot shapes and spacings. The exact modal series

solution should be used for small slot separations and the most accurate of the available asymptotic solutions for large slot separations. The computations by the two differenct methods should encompass overlapping regions for the specific slot configuration. The results could be tabulated for future reference in the design of arrays on curved surfaces.

Since mutual coupling for large slot separations can be computed only approximately at the present time, it is desirable to know the sensitivity of the slot admittance and null pattern on the calculated or measured admittance. It is felt that the sensitivity study can be performed by considering a planar array model of moderate size and lattice structure commensurate with one that would be used on a curved surface. This approach is most appropriate, since the planar array computer program is available and can be used to derive appropriate scattering coefficients.

REFERENCES

1. Bargeliotes, P. C., A.T. Villeneuve, and W. H. Kummer, 1975, Pattern Synthesis of Conformal Arrays, Final Report on Contract N00019-74-C0127, Hughes Aircraft Company, January 1974 to January 1975.

2. Bargeliotes, P. C., A. T. Vi-leneuve, and W. H. Kummer, 1976, Phased Array Antennas Scanned Near Endfire, Final Report on Contract N00019-75-C-0160, Hughes Aircraft Company, January 1975 to March 1976.

3. Golden, K. E., G. E. Stewart, and D. C. Pridmore-Brown, 1975, "Approximation Techniques for the Mutual Admittance of slot Antennas on Metallic Cones," IEEE Transactions on Antennas and Propagation, Vol. AP-22, January 1974, pp. 43-49.

4. Kummer, W. H., A. T. Villeneuve, and A. F. Seaton, 1973, Conformal Antenna Arrays Study, Final Report on Contract N00019-72-C-0212, Hughes Aircraft Company, Culver City, California, January 1972 to January 1973.

5. Lee, S. W., and R. Mittra, 1976, Study of Mutual Coupling Between Slots on a Cylinder, Final Report on Contract N00019-76-M-0622, Electromagnetics Laboratory, University of Illinois, Urbana, Ill., July 6, 1976 to November 15, 1976.

6. Hansen, R. V., "Circumferential Slot on Cylinder", Letter, September 1976.

APPENDIX

Because of the complex geometry of the conical array and the wide range of angles over which it is required to scan, it is necessary to have control over the polarization angle of the signal radiated by each element as well as the phase. If polarization control is not available, an excess amount of power will be lost into the cross-polarized signal at certain scan angles and certain angles of preferred polarization. Rotation of the angle of polarization of an element can be accomplished by controlling the amplitude of the signal fed to the two perpendicular arms of the element (assuming the element to be a crossed slot). If a circular waveguide element is used, then two orthogonal TE_{11} modes will need to be excited separately in the guide. A variable power divider with a range of zero to unity behind the element would be one approach to polarization control. However, in addition to the power divider, a 0 to 180-degree phase shifter would be required in one branch line to enable the polarization to be thrown into another quadrant. This geometry is illustrated in Figure A-1.

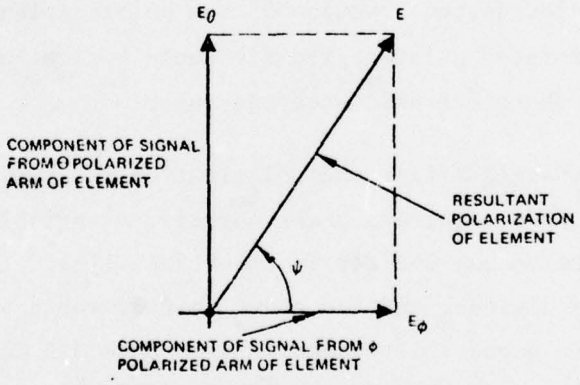

a. RESULTANT POLARIZATION IN 1ST QUADRANT

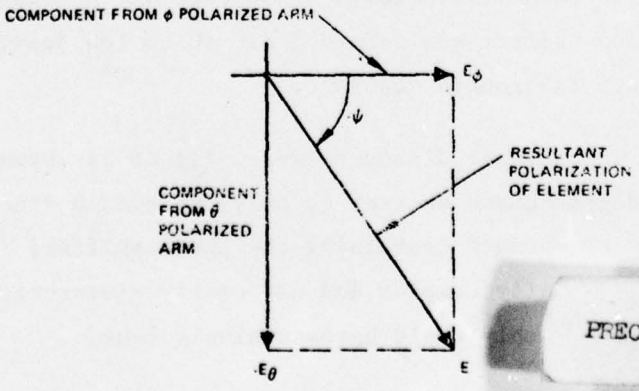

b. RESULTANT POLARIZATION IN 4TH QUADRANT

Figure A1. Geometry of Variable Polarization Elements.

It can be seen from Figure A-1a that a unity amplitude signal will be radiated at a polarization angle of ψ in the first quadrant if the two perpendicular components, E_ϕ and E_θ, have amplitudes of

$$E_\phi = E\cos\psi$$

$$E_\theta = E\sin\psi$$

Variation of the power uniformly from "all to the E_ϕ branch" to "all to the E_θ branch" will rotate the polarization throughout the quadrant. For the polarization to move into an adjacent quadrant, the sign of one of the components must be changed. Such a change is most easily done by a 180-degree phase shift of the signal in that branch. Figure A-1b shows the E_θ - component reversed in direction with the resultant polarization rotated into the fourth quadrant. The polarization does not have to be shifted into the other two quadrants because a 180-degree phase shift in the main signal line is equivalent to a 180-degree rotation of the polarization. A full range phase shifter that incorporates a 180-degree bit would be available in the main line to the element for the electronic steering function.

The complete phase-shifting and polarization-rotating system required for each element would thus require a phase shifter, a variable power divider, and a 0 to 180-degree phase shifter in one branch line. In practice, all components would be digital, and the phase shifter would probably be a 3-bit unit to give a phase shift capability of 0 to 315 degrees in 45-degree steps. The variable power divider would also be a 3-bit unit to provide polarization rotation capability from 0 to 90 degrees in steps of 22.5 degrees. The branch line phase shifter would have 1 bit (0 to 180 degrees) to shift the polarization into the fourth quadrant.

This assembly has several disadvantages: (1) it is asymmetrical (i.e., it has a 0 to 180-degree phase shifter in only one branch line); hence, losses would be greater in the branch containing the phase shifter; (2) variable power dividers are generally complex and not easily electronically controllable; and (3) the complete assembly would be excessively long.

Some of these objections can be overcome by combination of the phase-shifting and polarization-rotation functions into a single device. Such a device could consist of two hybrids separated by 3-bit phase shifters as shown in Figure A-2. Each 3-bit phase shifter would have eight states. For each state of one of the phase shifters, the other could assume any one of its eight states, so that the device would have a total of 64 states. It can

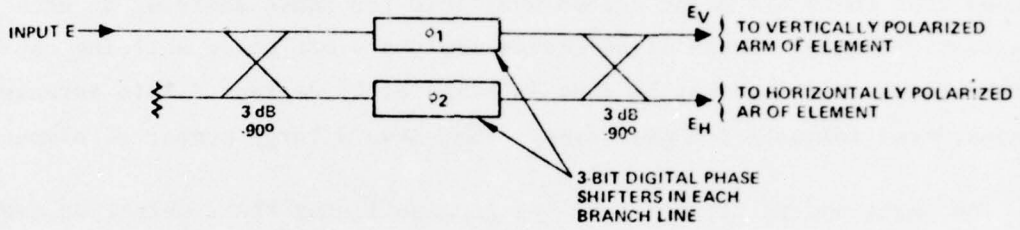

Figure A-2. Combined digital phase-shifter/polarization-rotator for conical phased array.

be shown that the two output signals of this device would be either exactly in-phase with each other or exactly 180 degrees out-of-phase regardless of the settings of the phase shifters. As a result, all the states would generate linearly polarized waves when the outputs were connected to orthogonal terminals of a radiator.

It is desirable that the polarization be stepped in relatively small steps so that the cross-polarized component will remain low. With 22.5-degree steps, the largest polarization error is 11.25 degrees, which puts the maximum cross-polarized component from any one element 14.2 dB below the preferred component. On the average it will be on the order of 20 dB down. If the polarization had to be stepped entirely around the 360-degree circle in 22.5-degree steps, 16 positions would be required implying a 4-bit polarization-rotator. However, as discussed above, half of these states can be obtained by a 180-degree phase shift and are thus redundant. It will be satisfactory if the combined phase-

shifter/polarization-rotator rotates the phase between -67.5 degrees and +90 degrees in ψ in 22.5-degree steps. This rotation requires eight positions and hence uses up 8 of the 64 states available from the device. Since a certain number of bits of phase shift control is required for each polarization angle, the total number of states required is the product of the number of states specified for phase shifting and the number of states required for polarization rotation. With 8 states allocated to polarization rotation, this implies that there are eight states available for phase shifting at each polarization angle. These eight states imply a 3-bit phase shifting capability so that phase shifting must be done in steps of 45 degrees. This arrangement is considered adequate for most arrays that have a large number of elements.

The phase and polarization states available from the combination device are given Table A-I. As can be seen, the phase states available shift by 22.5 degrees between adjacent polarization states. For a planar phased array, this shift is no problem because all elements would have the same polarization angle at any one time. In the conformal phased array, an effect will be noticed at some scan angles when some of the elements will need to be rotated to slightly different polarization angles in relation to the geometry of the surface to obtain the lowest cross-polarized component at the beam peak.

TABLE A-I. PHASE AND POLARIZATION STATES AVAILABLE FROM THE PHASE-SHIFTER/POLARIZATION-ROTATOR

Phase	Polarization Angle, ψ							
	-67.5°	-45°	-22.5°	0°	22.5°	45°	67.5°	90°
-157.5	0, 135		45, 90		90, 45		135, 0	
-135.0		0, 90		45, 45		90, 0		135, 315
-112.5	315, 90		0, 45		45, 0		90, 315	
-90.0		315, 45		0, 0		45, 315		90, 270
-67.5	270, 45		315, 0		0, 315		45, 270	
-45.0		270, 0		315, 315		0, 270		45, 225
-22.5	225, 0		270, 315		315, 270		0, 225	
0.0		225, 315		270, 270		315, 225		0, 180
22.5	180, 315		225, 270		270, 225		315, 180	
45.0		180, 270		225, 225		270, 180		315, 135
67.5	135, 270		180, 225		225, 180		270, 135	
90.0		135, 225		180, 180		225, 135		270, 90
112.5	90, 225		135, 180		180, 135		225, 90	
135.0		90, 180		135, 135		180, 90		225, 45
157.5	45, 180		90, 135		135, 90		180, 45	
180.0		45, 135		90, 90		135, 45		180, 0

NOTE: The numbers at each location refer to the phase-shifter settings required to obtain the indicated phase and polarization angle. The first number is for the phase shifter in the upper line, and the second for the lower (in Figure A-2).

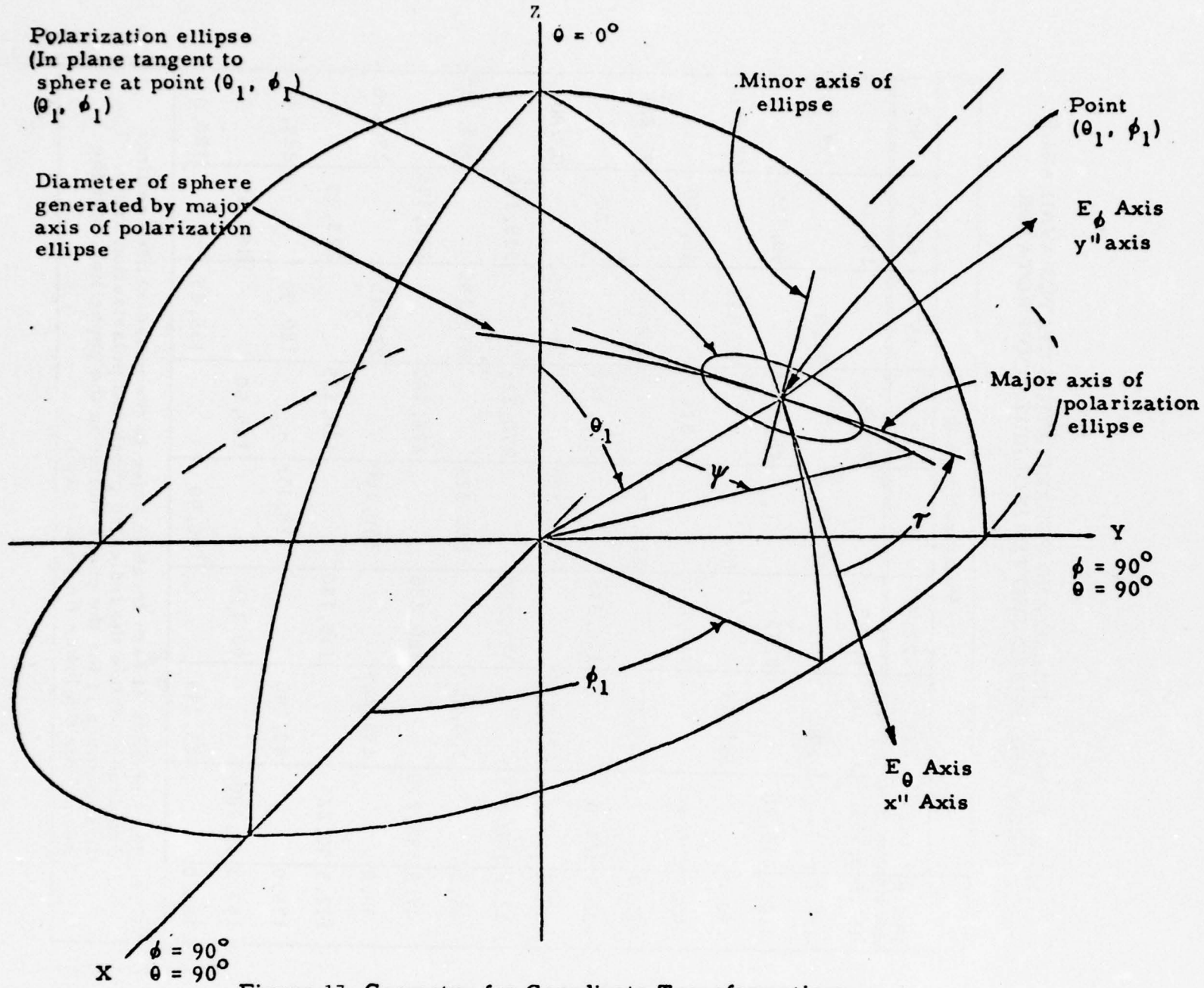

Figure 17. Geometry for Coordinate Transformations

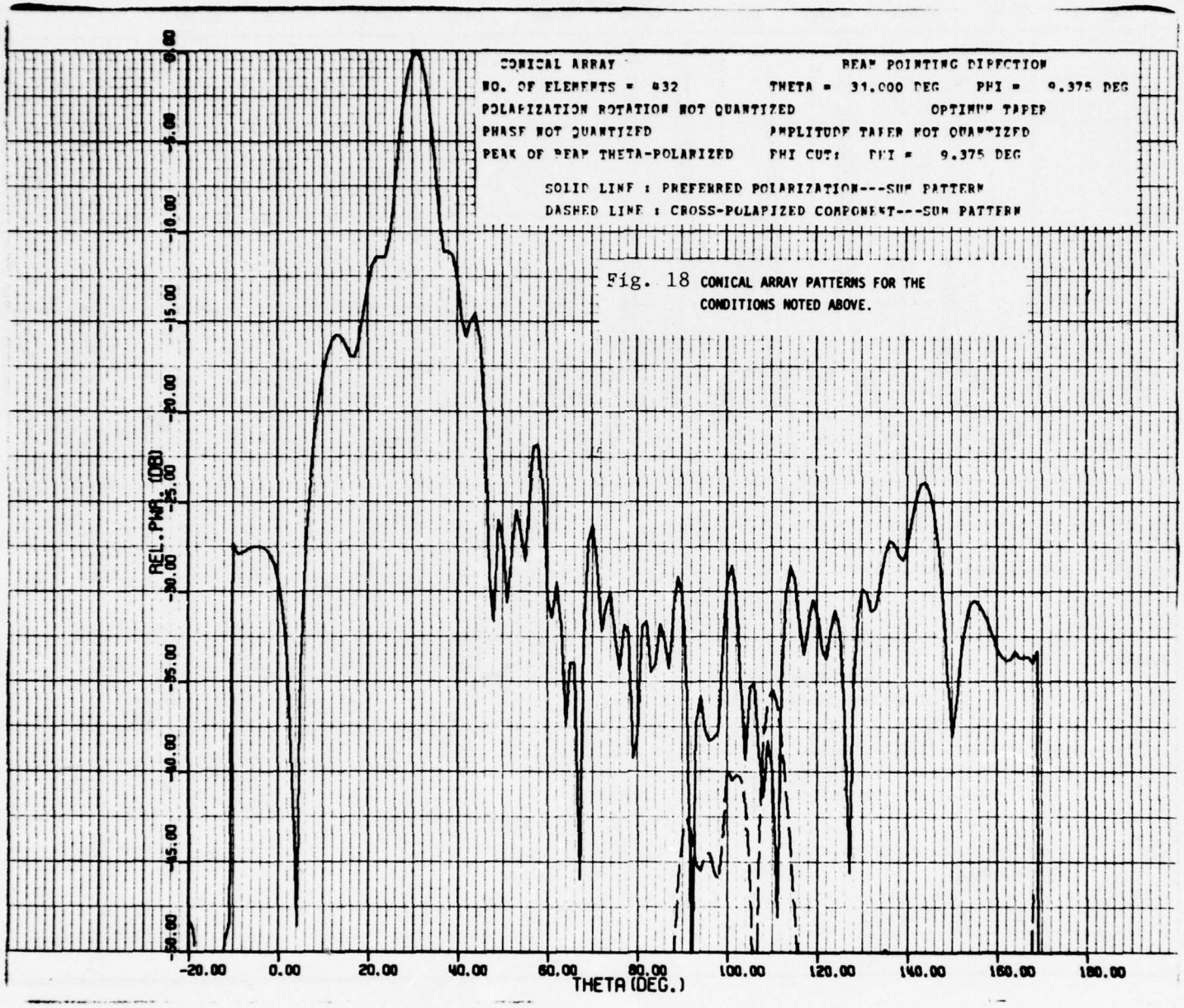

Fig. 18 CONICAL ARRAY PATTERNS FOR THE CONDITIONS NOTED ABOVE.

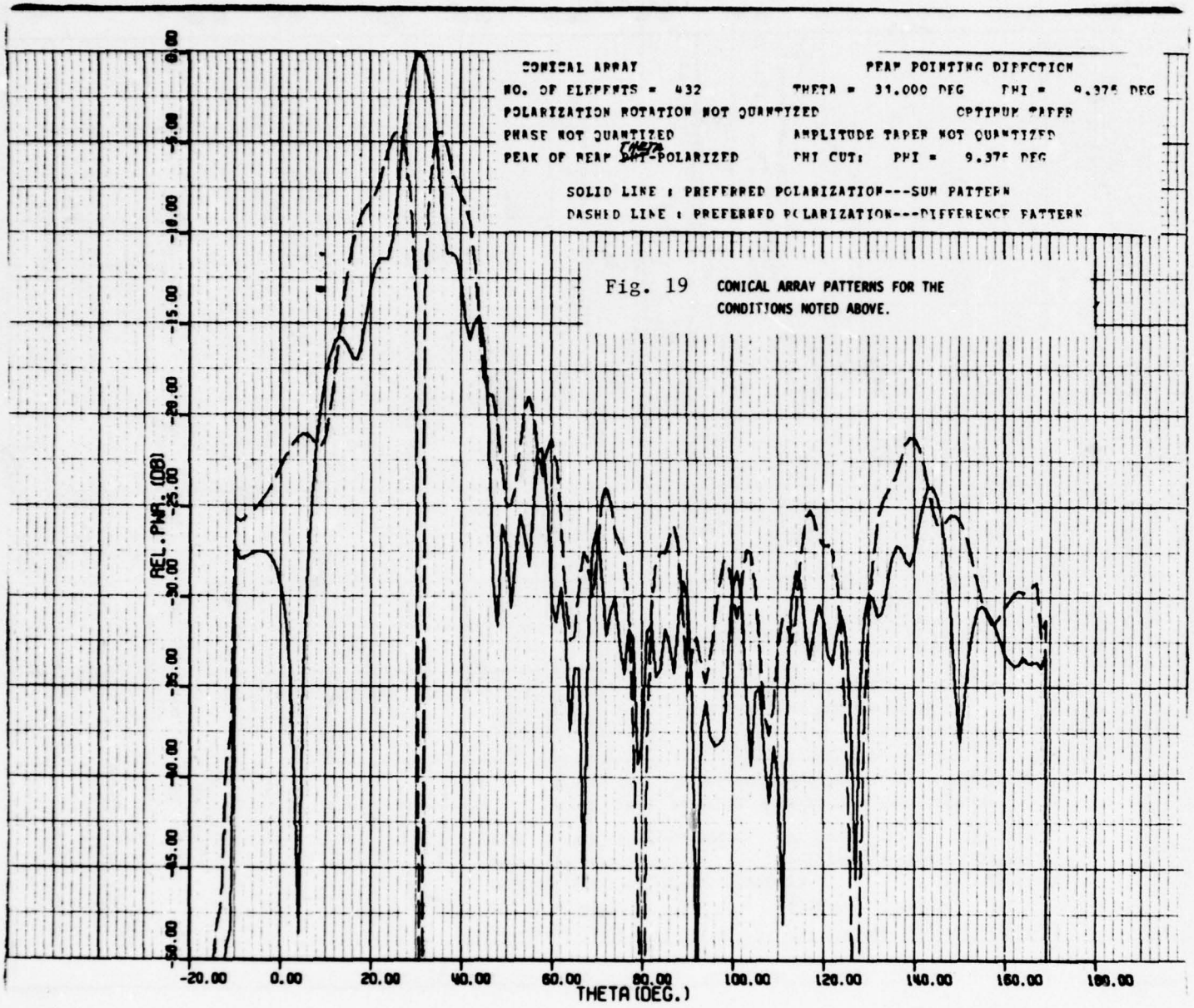

Fig. 19 CONICAL ARRAY PATTERNS FOR THE CONDITIONS NOTED ABOVE.

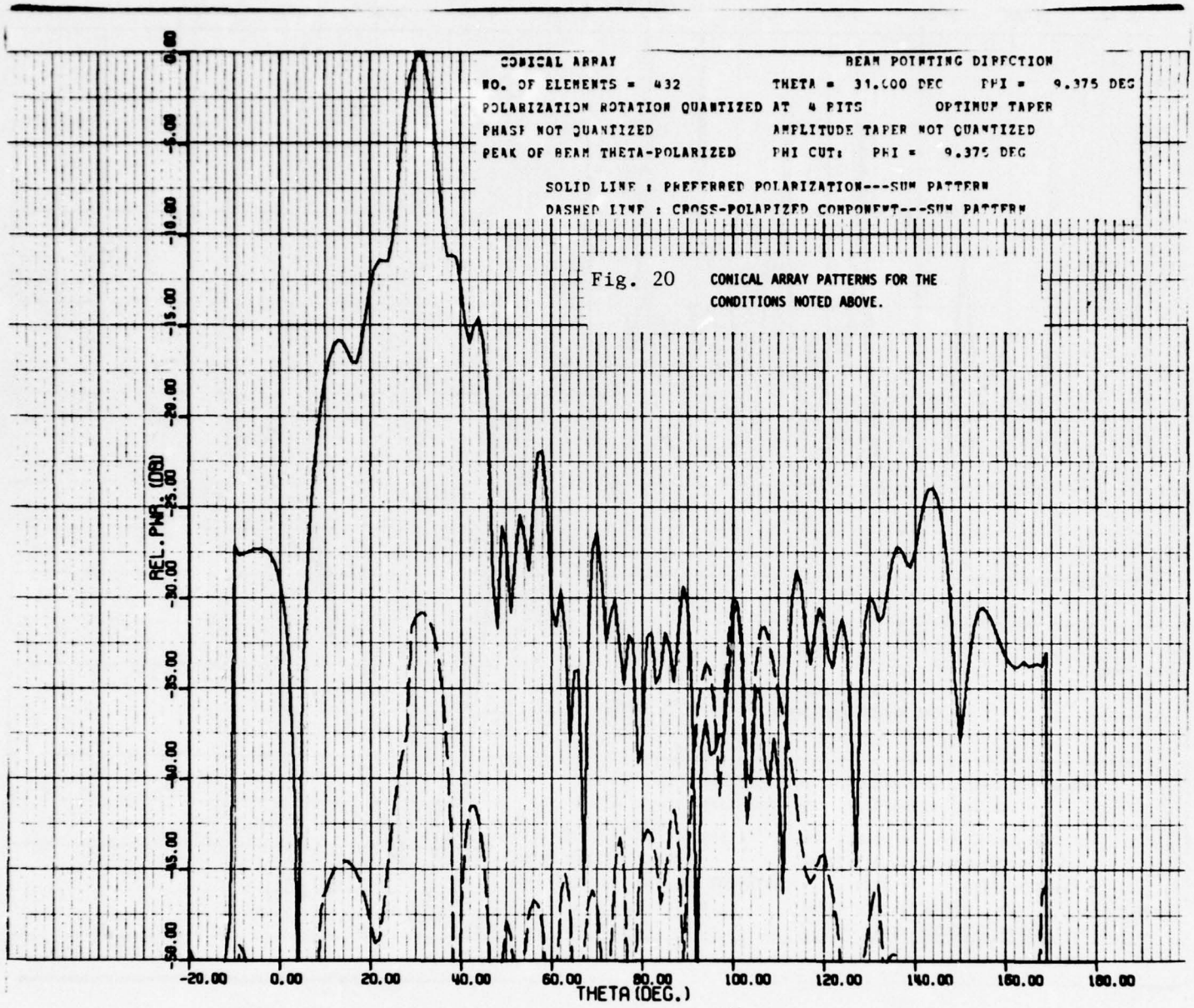

Fig. 20 CONICAL ARRAY PATTERNS FOR THE CONDITIONS NOTED ABOVE.

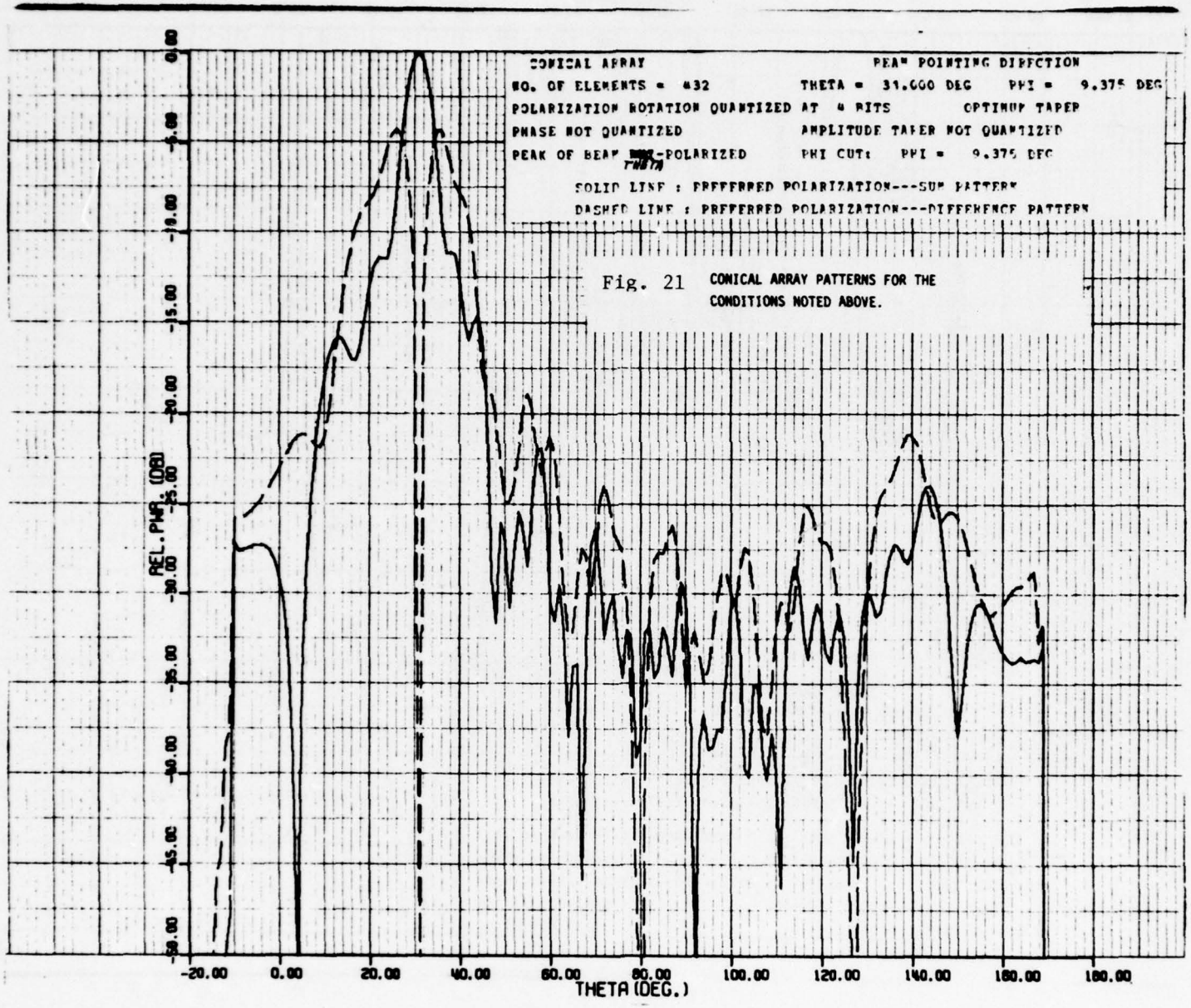

Fig. 21 CONICAL ARRAY PATTERNS FOR THE CONDITIONS NOTED ABOVE.

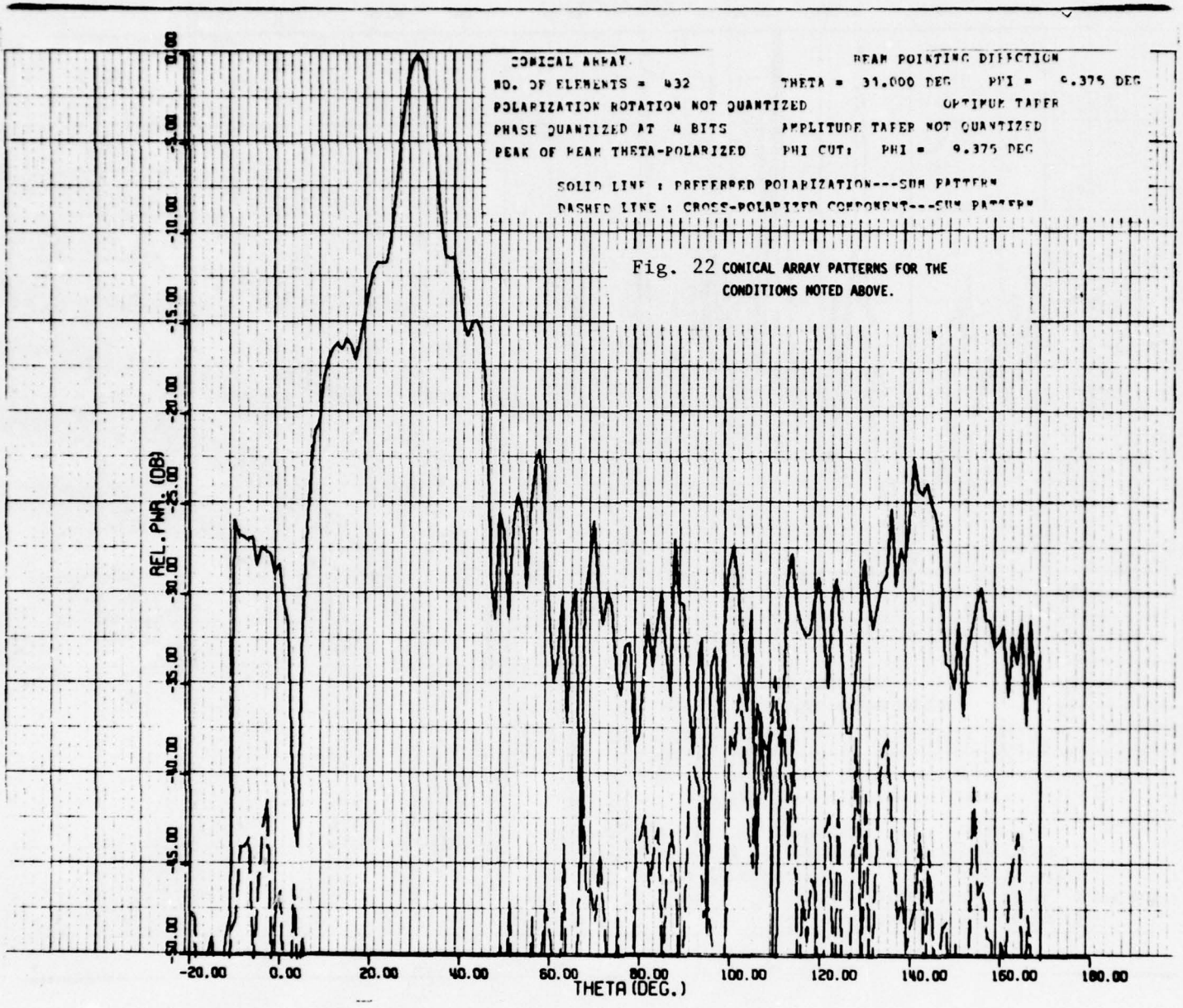

Fig. 22 CONICAL ARRAY PATTERNS FOR THE CONDITIONS NOTED ABOVE.

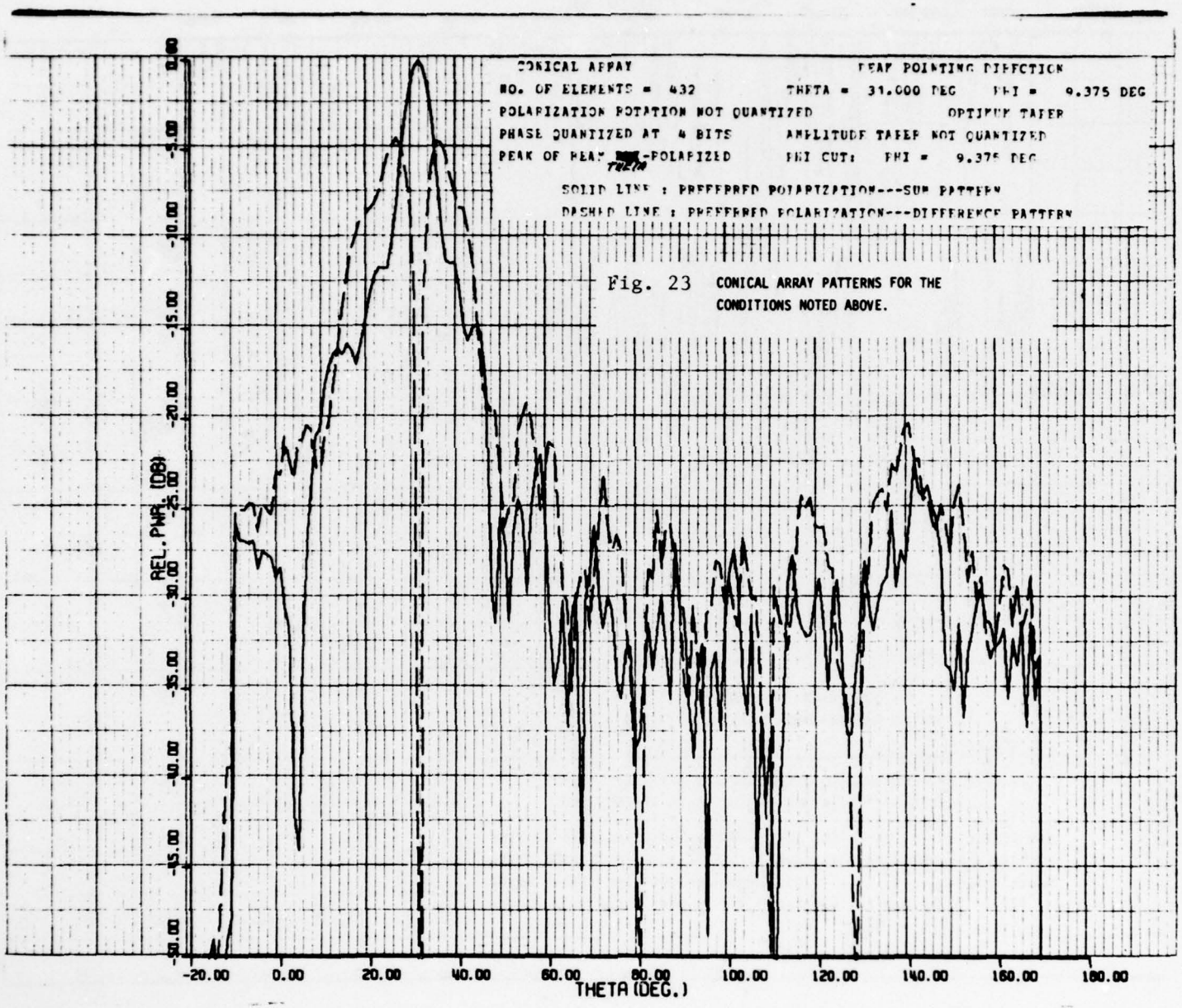

Fig. 23 CONICAL ARRAY PATTERNS FOR THE CONDITIONS NOTED ABOVE.

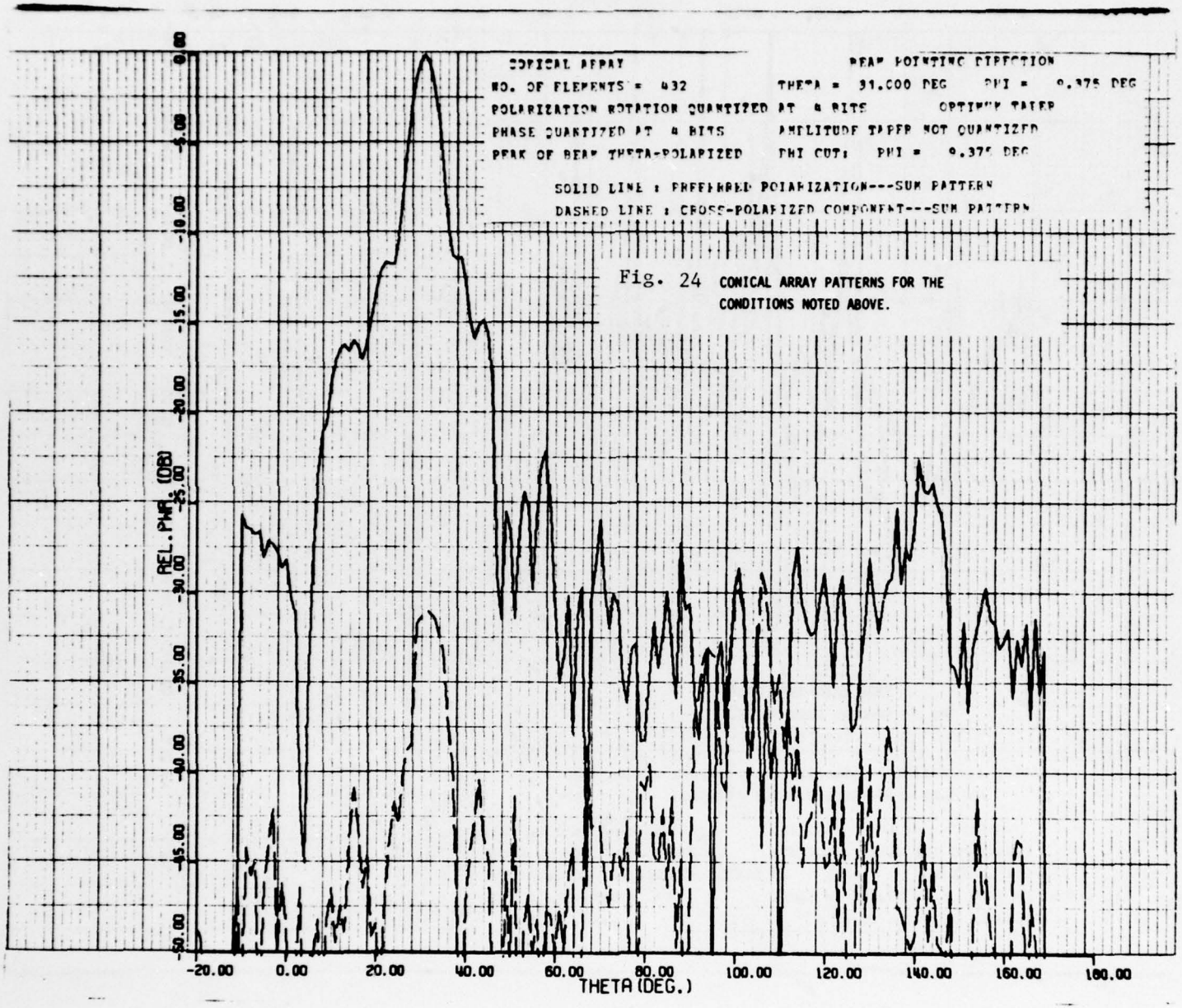

Fig. 24 CONICAL ARRAY PATTERNS FOR THE CONDITIONS NOTED ABOVE.

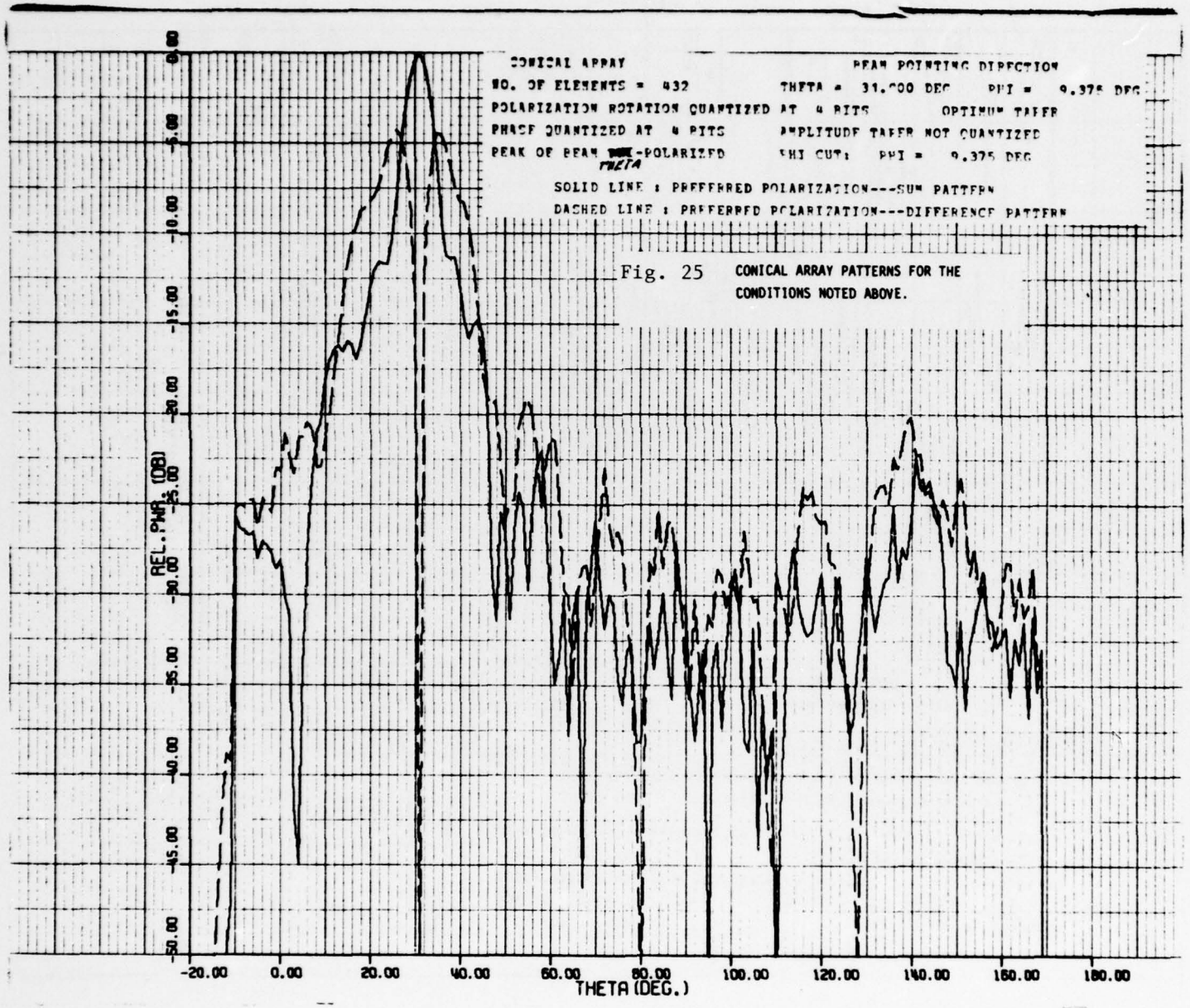

Fig. 25 CONICAL ARRAY PATTERNS FOR THE CONDITIONS NOTED ABOVE.

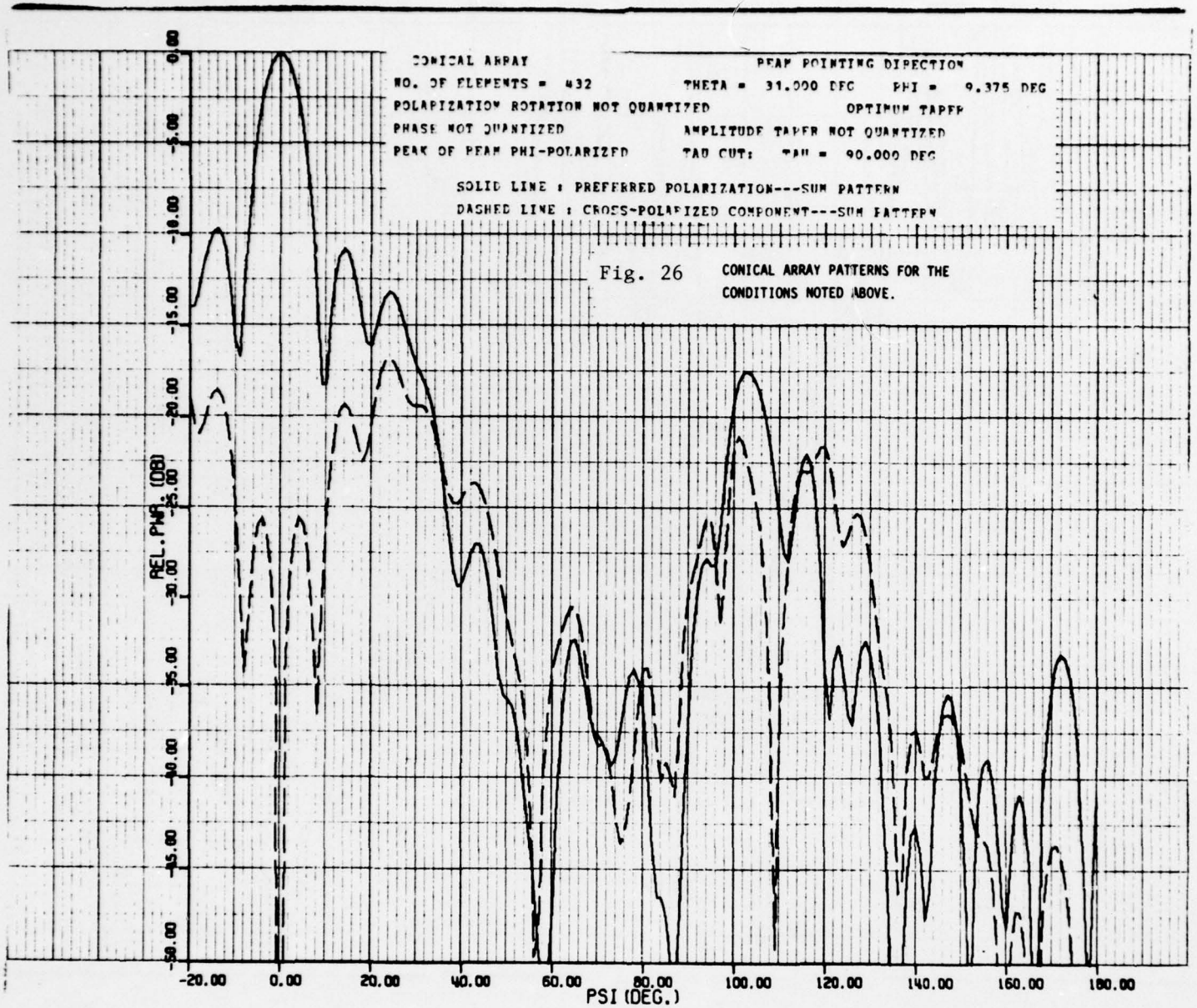

Fig. 26 CONICAL ARRAY PATTERNS FOR THE CONDITIONS NOTED ABOVE.

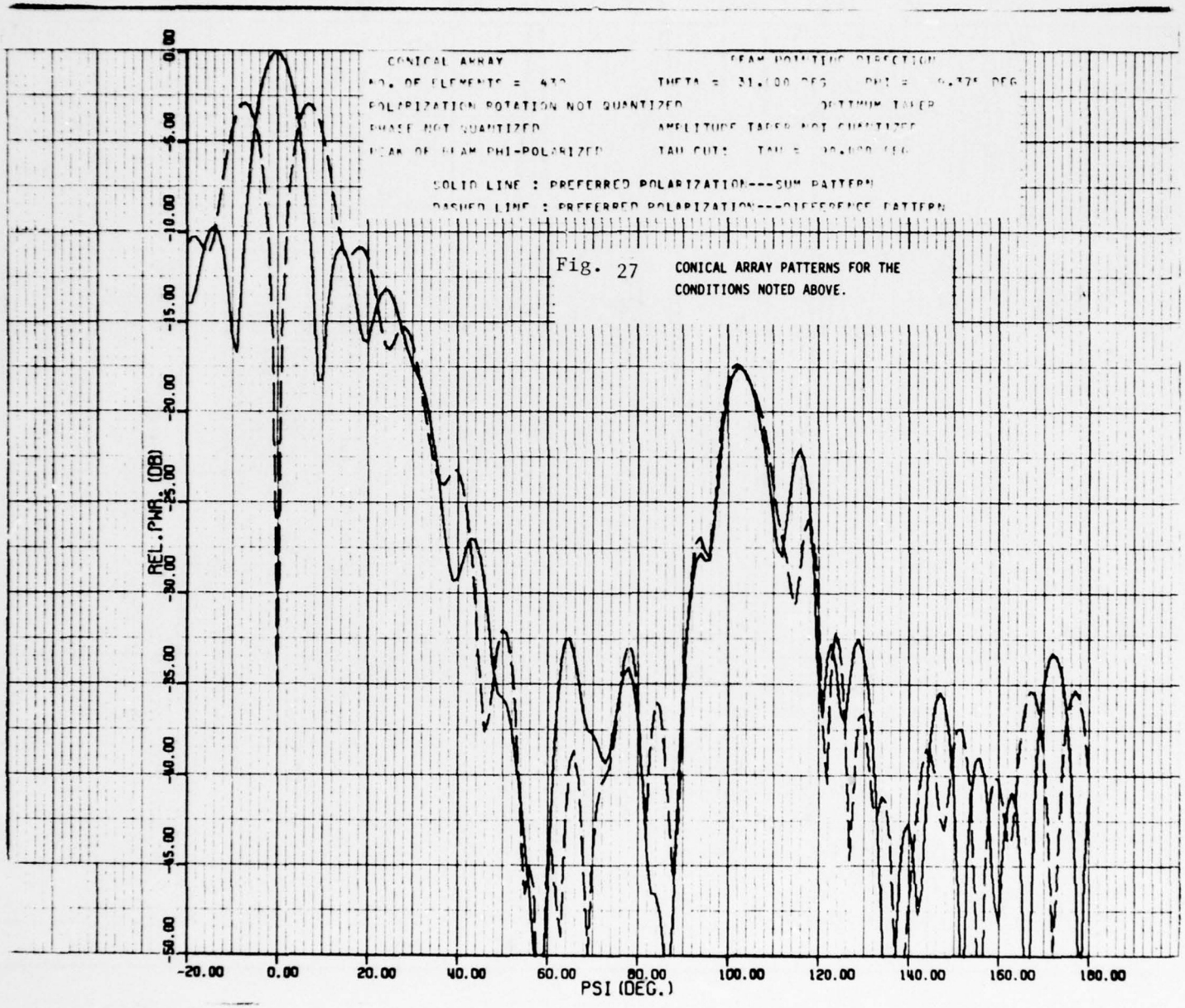

Fig. 27 CONICAL ARRAY PATTERNS FOR THE CONDITIONS NOTED ABOVE.

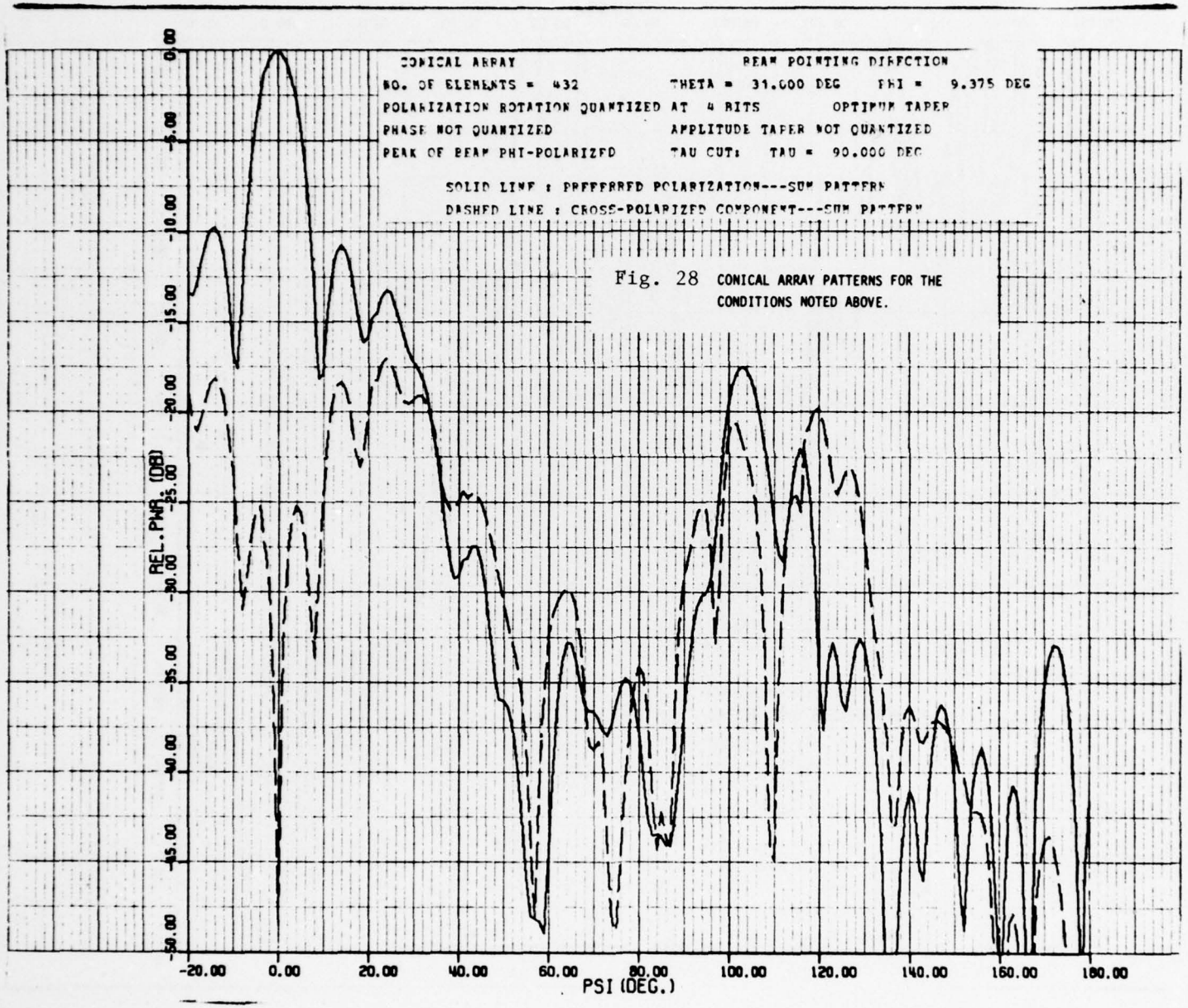

Fig. 28 CONICAL ARRAY PATTERNS FOR THE CONDITIONS NOTED ABOVE.

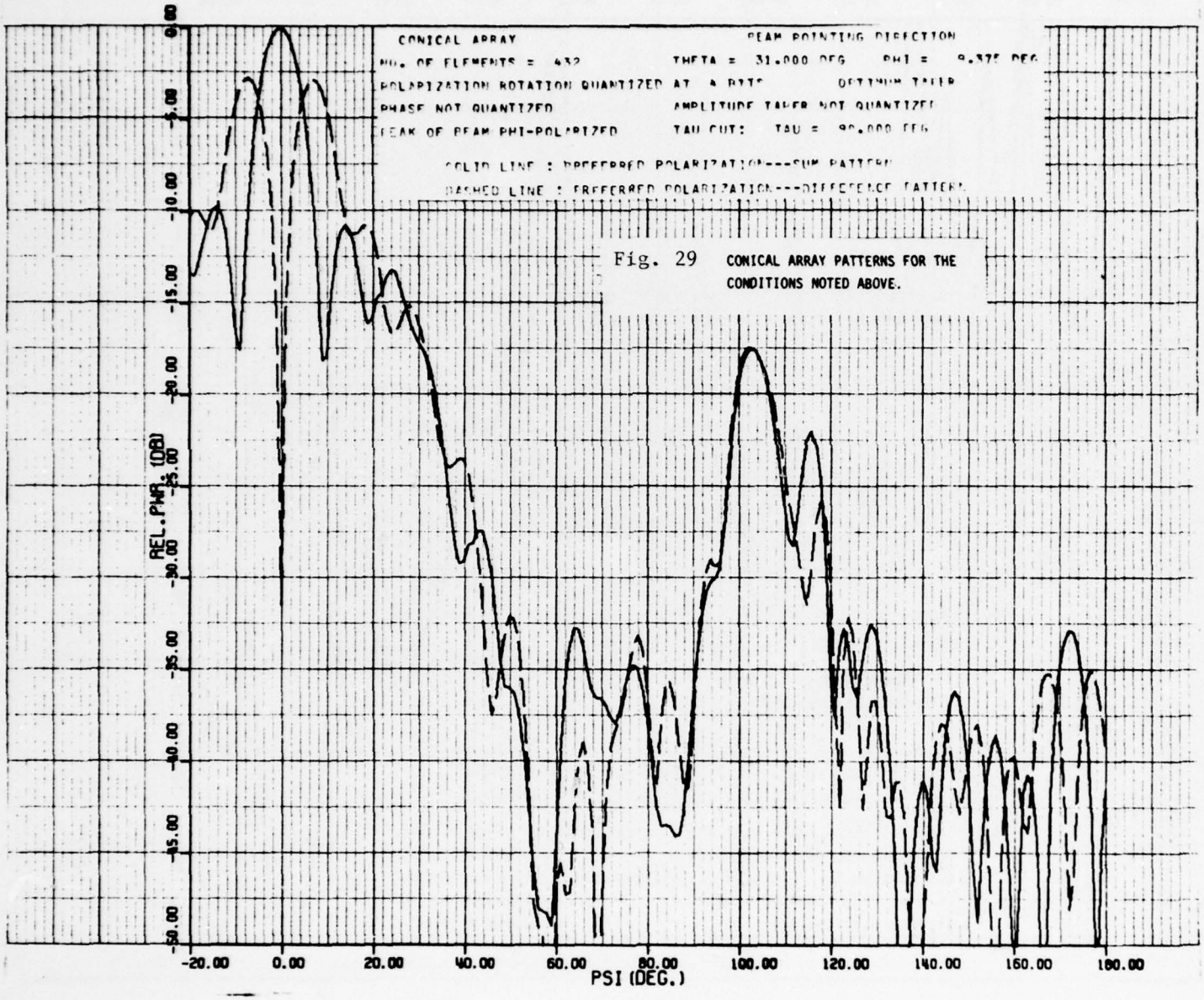

Fig. 29 CONICAL ARRAY PATTERNS FOR THE CONDITIONS NOTED ABOVE.

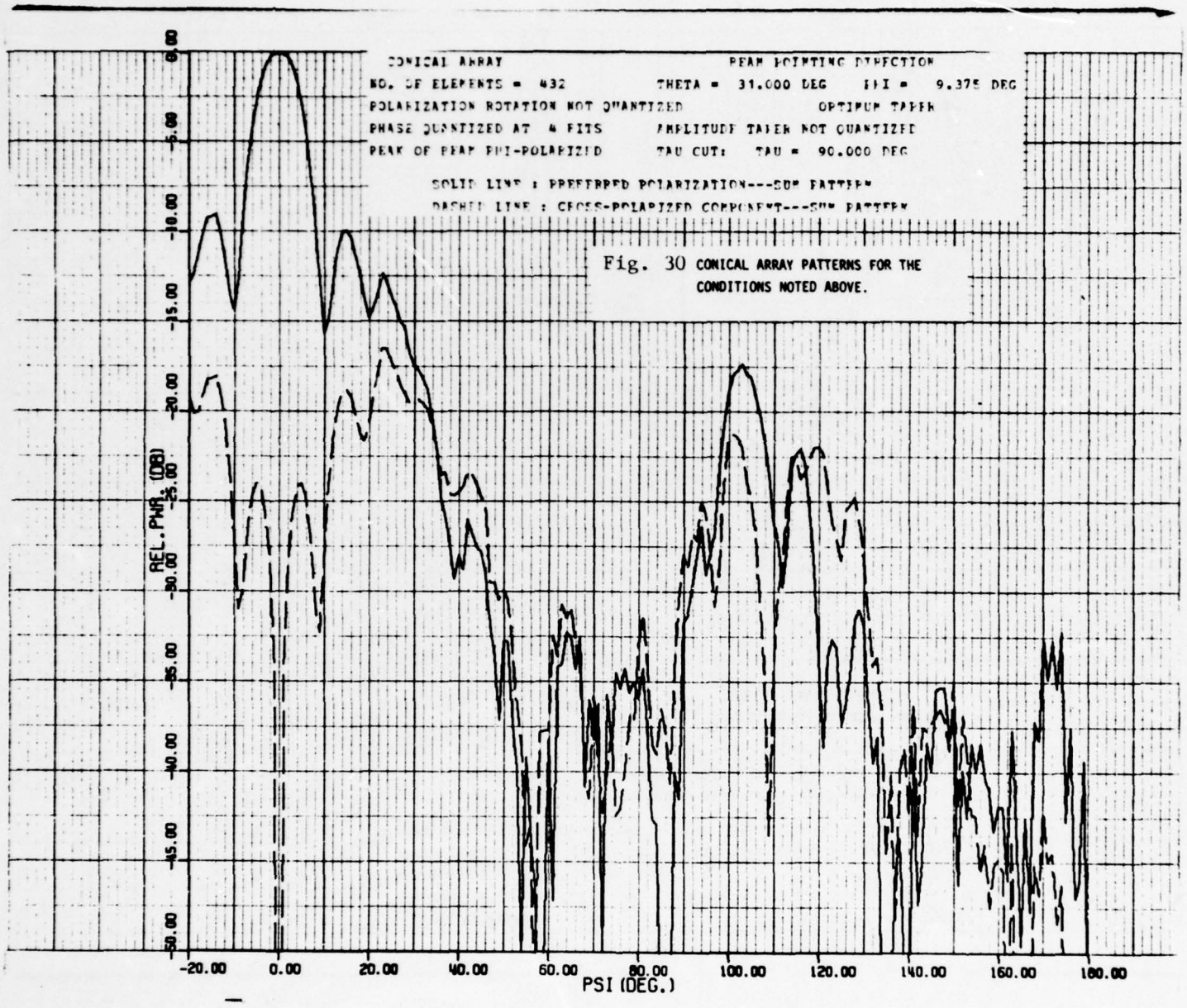

Fig. 30 CONICAL ARRAY PATTERNS FOR THE CONDITIONS NOTED ABOVE.

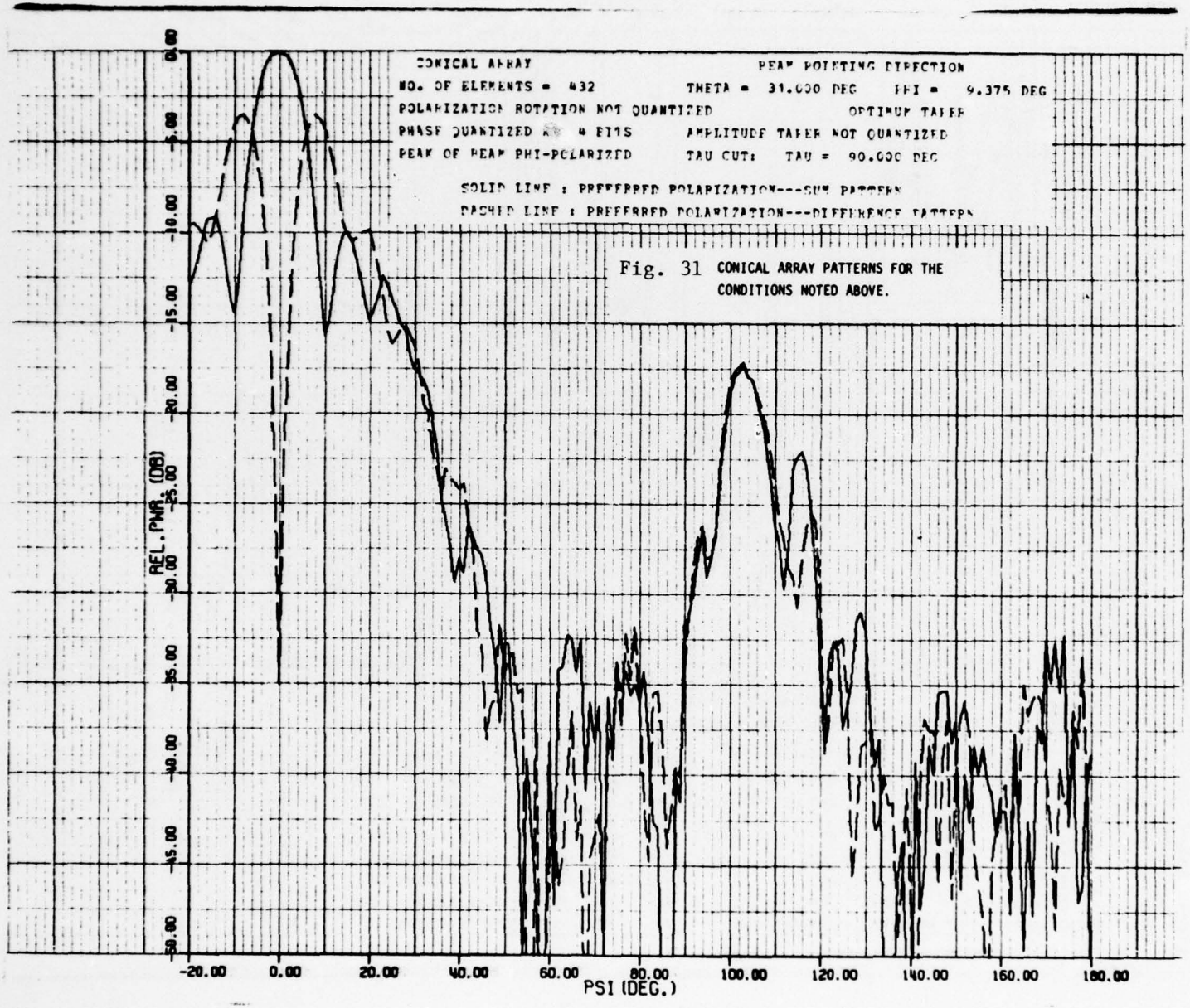

Fig. 31 CONICAL ARRAY PATTERNS FOR THE CONDITIONS NOTED ABOVE.

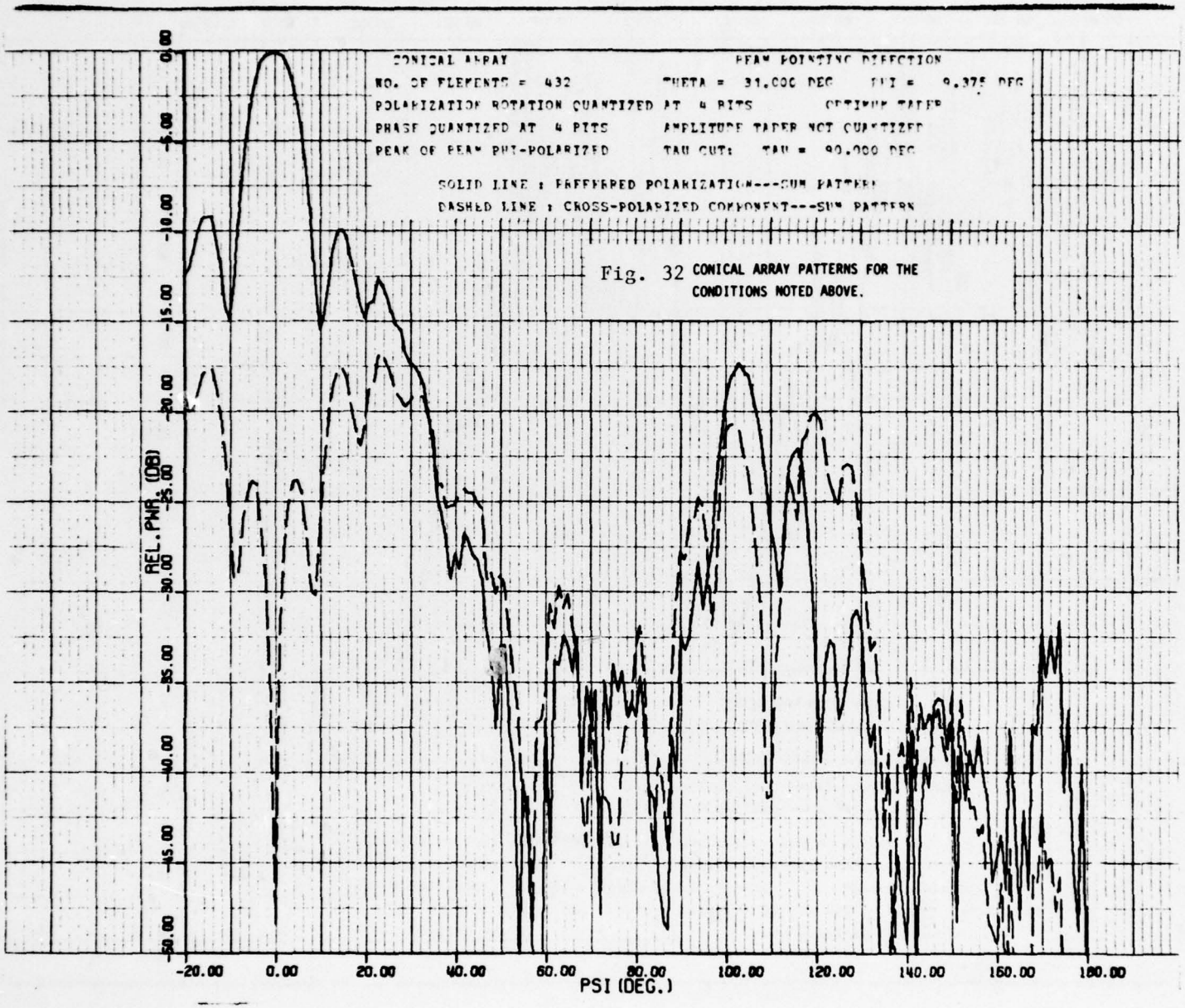

Fig. 32 CONICAL ARRAY PATTERNS FOR THE CONDITIONS NOTED ABOVE.

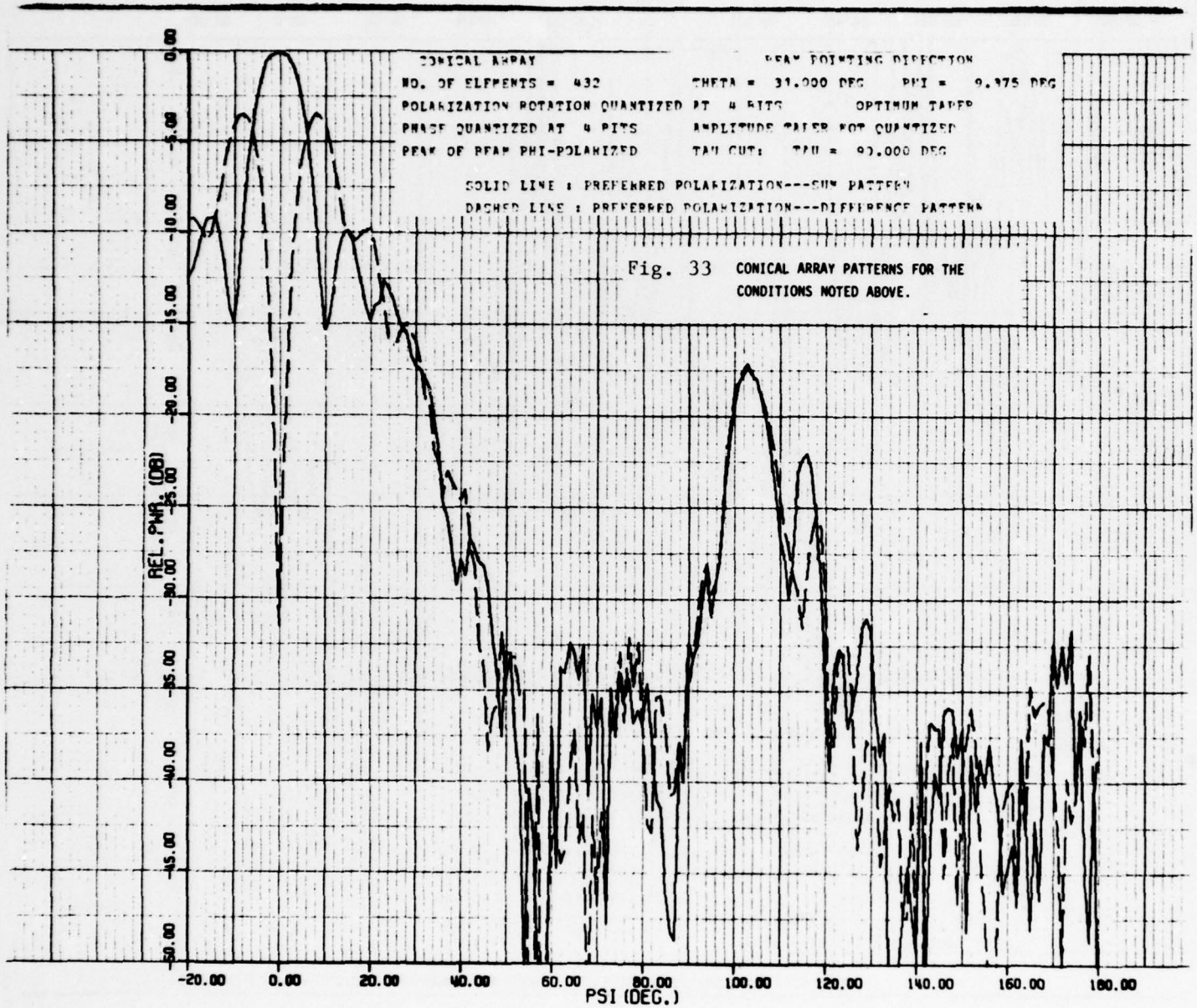

Fig. 33 CONICAL ARRAY PATTERNS FOR THE CONDITIONS NOTED ABOVE.

DISTRIBUTION

Commander
Naval Air Systems Command
Department of the Navy
Washington, D.C. 20360
Attn: AIR-53321A
AIR-360
AIR-50174 (14 cys./Final only)
AIR-310B (2/Quart. -5 Final)

Commander
Naval Ordnance Systems Command
Department of the Navy
Washington, D.C. 20360
Attn: NSEA-0341

Director
Office of Naval Research
800 North Quincy Street
Arlington, Virginia 22217
Attn: ONR-427

Raytheon Company
Missile Systems Division
Hartwell Road
Bedford, Massachusetts 01730
Attn: Mr. Walter Jeros,
MS S2-32

Commander
Air Force Avionics Laboratory
Electronic Warfare Division
Wright-Patterson Air Force Base
Ohio 45433
Attn: Mr. Harold Weber

Commanding Officer
Naval Air Development Center
Radar Division
Warminster, Pennsylvanis 18974
Attn: Mr. J. B. Lyons, Code 204

Director
Naval Research Laboratory
Washington, D.C. 20390
Attn: Code 5360
Code 5350
Code 5368
Code 5330

Commanding Officer
Naval Avionics Facility
Indianapolis, Indiana 46218
Attn: Mr. Paul Brink

Commander
Naval Electronics Laboratory Center
San Diego, California 92152
Attn: Mr. J. Provencher, Code 2330

General Dynamics
Electronics Division
P. O. Box 81127
San Diego, California 92138
Attn: Dr. G. Tricoles

Director
Electro-Sciences Laboratory
Ohio State University
1320 Kinnear Road
Columbus, Ohio 43212
Attn: Mr. Robert Fouty

Sperry-Rand Corporation
Sperry Gyroscope Division
Microwave Engineering Department
Great Neck, New York 11020
Attn: Dr. Robert J. Tims

ETE
Hanscom Air Force Base
Bedford, Massachusetts 07130
Attn: Mr. Philip Blacksmith/ETER

McDonnel Douglas Astronautics Co.
5301 Bolsa Avenue
Huntington Beach, California 92647
Attn: Mr. John Wright/Mail Stop 9
Department A3-830/BB10

Teledyne Ryan Company
5650 Kearny Mesa Road
San Diego, California 92119
Attn: Mr. H. Penner

Teledyne Micronetics
7155 Mission Gorge Rd.
San Diego, California 92120
Attn: Dr. S. Weisbrod

DISTRIBUTION - Continued

Advanced Sensor Laboratory
U.S. Army Missile Command
Redstone Arsenal
Huntsville, Alabama 35809
Attn: Mr. W. Lindberg/DRSMI-RE

Harry Diamond Laboratories
2800 Powder Mill Road
Adelphi, Maryland 20783
Attn: Dr. Howard S. Jones, Jr./
AMXDO-RAE

Dr. John K. Smith (Code 2042)
Naval Air Development Center
Warminister, Pennsylvania 18974

Dr. Alex Hessel
Polytechnic Institute of New York
Route 110
Farmingdale, L.I., N.Y. 11735

U.S. Army Electronics Command
CS and TA Laboratory
DRSEL-CT-R
Fort Monmouth, N.J. 07703
Attn: Mr. Boaz Gelernter

Missile Intelligence Agency
U.S. Army Missile Command
Redstone Arsenal
Huntsville, Alabama 35809
Attn: Mr. R. Thompson
(AMSMI/YPE)

ADTC/DLMI
Eglin Air Force Base
Florida 32542
Attn: T. Aden
D. Edwards

Dr. R. C. Hansen
P.O. Box 215
Tarzana, California 91356

University of Illinois
Department of Electrical Engineering
Electromagnetics Laboratory
Urbana, Illinois 61801
Attn: Dr. S. W. Lee

SAMSO
Los Angeles Air Force Station
P.O. Box 92960
Los Angeles, California 90009
Attn: Lt. J. D. Rouge/RSMG

Aerospace Corporation
Building 105
P.O. Box 95085
Los Angeles, California 90045
Attn: Paul Sokoloff

Dr. Gordon E. Stewart
Aerospace Corporation
Bldg. 120, M/S 2031
P.O. Box 92957
Los Angeles, California 90009

Unclassified

SECURITY CLASSIFICATION OF THIS PAGE (When Data Entered)

REPORT DOCUMENTATION PAGE		READ INSTRUCTIONS BEFORE COMPLETING FORM
1. REPORT NUMBER	2. GOVT ACCESSION NO.	3. RECIPIENT'S CATALOG NUMBER
4. TITLE (and Subtitle) Conformal Phased Array Breadboard		5. TYPE OF REPORT & PERIOD COVERED Final Report, January 1977
		6. PERFORMING ORG. REPORT NUMBER 2753/981, HAC-Ref. No. D6190
7. AUTHOR(s) Peter C. Bargeliotes, A.F. Seaton, Alfred T. Villeneuve, Wolfgang H. Kummer		8. CONTRACT OR GRANT NUMBER(s) N00019-76-C-0495
9. PERFORMING ORGANIZATION NAME AND ADDRESS Hughes Aircraft Company Culver City, California 90230		10. PROGRAM ELEMENT, PROJECT, TASK AREA & WORK UNIT NUMBERS 84 p.
11. CONTROLLING OFFICE NAME AND ADDRESS Air Systems Command Department of the Navy Washington, D.C.		12. REPORT DATE January 1977
		13. NUMBER OF PAGES 80
14. MONITORING AGENCY NAME & ADDRESS (if different from Controlling Office)		15. SECURITY CLASS. (of this report) Unclassified
		15a. DECLASSIFICATION/DOWNGRADING SCHEDULE

16. DISTRIBUTION STATEMENT (of this Report)

Distribution limited to U.S. Agencies only; test and evaluation (January 1977); other requests for this document must be referred to Commander, Naval Air Systems Command, AIR-310B, Washington, D. C. 20360

APPROVED FOR PUBLIC RELEASE: DISTRIBUTION UNLIMITED

17. DISTRIBUTION STATEMENT (of the abstract entered in Block 20, if different from Report)

18. SUPPLEMENTARY NOTES

19. KEY WORDS (Continue on reverse side if necessary and identify by block number)

Antenna, conformal, conical, array, element, pattern, synthesis, slot, modal series, optical, transition, diffraction, scattering, contour, asymptotic, equivalence principle, quantization, polarization, admittance, mutual admittance, coupling, phase shifter, computer programs.

20. ABSTRACT (Continue on reverse side if necessary and identify by block number)

Flush mounted slot antenna systems on metallic cones or ogival surfaces can be inertialessly scanned in the required direction. Since scanning over a wide angular region is generally desired, the radiation characteristics, including the effect of mutual coupling on the radiating elements, must be investigated before the more detailed system aspects are considered. To this end, various approximation techniques have been examined for use in pattern calculations and in impedance calculations. These include the approximate asymptotic approach

(Continued)

OVER

DD FORM 1 JAN 73 1473 EDITION OF 1 NOV 65 IS OBSOLETE

Unclassified

SECURITY CLASSIFICATION OF THIS PAGE (When Data Entered)

402 429

and the equivalence principle technique. The approximation techniques provide simplified computations as compared with the exact technique, and are not applicable to all conditions. A combination of exact and approximation techniques is generally required to design or analyze an array.

The approximate asymptotic approach, which allows the separation of the diffracted field and geometrical optics fields, has been examined in detail. It appears that the asymptotic representation of the Legendre function chosen for the analysis leads to divergent expressions as the mode number m is increased, and hence limits the usefulness of the asymptotic approach in the present problem. The divergent nature of the asymptotic expression is verified by computed radiation patterns of several azimuthal modes.

A computer program is being developed to apply the equivalence principle technique to a conical surface. The new program will employ an improved element pattern over previous versions with an array lattice identical to that used by the companion program for phase and polarization quantization. Preliminary computed patterns show that degradation due to quantization of the polarization-rotation and phase shift is not severe. In addition, mutual admittance calculations of slots on a cylinder have been made using the harmonic series solution. The cylinder is taken as the test model for other configurations, since the harmonic series results in precise calculations of mutual coupling for the cylinder. These calculations have been used to check the accuracy of an alternative modal solution which can be used to compute mutual admittance between slots with large axial separation.